KfK 3994
Dezember 1985

Comparison of High Temperature Steam Oxidation Behavior of Zircaloy-4 versus Austenitic and Ferritic Steels under Light Water Reactor Safety Aspects

S. Leistikow, G. Schanz, Z. Zurek
Institut für Material- und Festkörperforschung
Projekt Nukleare Sicherheit

Kernforschungszentrum Karlsruhe

KERNFORSCHUNGSZENTRUM KARLSRUHE

Institut für Material- und Festkörperforschung
Projekt Nukleare Sicherheit

KfK 3994

Comparison of High Temperature Steam Oxidation Behavior of Zircaloy-4 versus Austenitic and Ferritic Steels under Light Water Reactor Safety Aspects[+)]

S. Leistikow, G. Schanz, Z. Zurek[x]

[x]Formerly Guest Scientist of
Techn. University of Cracow (Poland)
Institute of Inorganic Chemistry and Technology

[+)]Paper presented to the Polish-German Seminar on "Properties of High Temperature Alloys", Cracow, Poland; July3-6, 1985

Kernforschungszentrum Karlsruhe GmbH, Karlsruhe

Kernforschungszentrum Karlsruhe GmbH
Postfach 3640, 7500 Karlsruhe 1

ISSN 0303-4003

Abstract

A comparative study of the oxidation behavior of Zircaloy-4 versus ferritic-martensitic steel No. 1.4914 and austenitic stainless steel No. 1.4970 was performed in high temperature steam. Nuclear reactor typical tube sections of all three materials were exposed on both sides to superheated steam at temperatures ranging from 600 to 1300°C for up to 6 h. The specimens were evaluated by gravimetry, metallography, and other methods. The results are presented in terms of weight gain, corresponding metal (wall) penetration and consumption as function of time and temperature.

Concerning the corrosion resistance the ranking position of Zircaloy-4 was between the austenitic and the ferritic steel. Because of the chosen wall dimensions Zircaloy-4 and the austenitic steel behaved similarly in that the faster oxidation of the thicker Zircaloy-4 cladding consumed the total wall thickness in a time equivalent to the slower oxidation of the thinner austenitic steel cladding. The ferritic steel cladding however was faster consumed because of the lower oxidation resistance and the thinner wall thickness compared to the austenitic steel. So besides oxide scale formation, oxygen diffusion into the bulk of the metal forming various oxygen-containing phases were evaluated - also in respect to their influence on mechanical cladding properties and the dimensional changes.

Vergleich des Hochtemperatur-Oxidationsverhalten von Zircaloy-4 mit austenitischen und ferritischen Stählen unter Leichtwasserreaktor - Sicherheitsaspekten

Zusammenfassung

Eine vergleichende Untersuchung über das Oxidationsverhalten von Zircaloy-4 sowie das eines ferritisch-martensitischen Stahls (Werkstoff Nr. 1.4914) und eines austenitischen Stahls (Werkstoff Nr. 1.4970) wurde in Hochtemperatur-Dampf durchgeführt. Dazu wurden als Proben kernreaktortypische Rohrabschnitte aller drei Materialien beidseitig dem überhitzten Wasserdampf bei Temperaturen von 600-1300°C und Zeiten bis zu 6 Stunden exponiert. Die Proben wurden durch Gravimetrie, Metallographie und Einsatz anderer Methoden ausgewertet. Die Ergebnisse werden als Gewichtszunahme sowie der ihr entsprechenden Metall-(Wand-)Durchdringung oder Metallumsatz in Funktion von Zeit und Temperatur dargestellt.

Bezüglich der Korrosionsbeständigkeit der Rohrmaterialien wurde die Position des Zircaloy-4 als zwischen dem beständigeren austenitischen und dem unbeständigeren ferritischen Stahl gelegen befunden. Aufgrund der gewählten Rohrabmessungen wurde eine Übereinstimmung des Verhaltens von Zircaloy-4 und dem austenitischen Stahl dahingehend gefunden, daß die schnellere Oxidation des dickeren Zircaloy-4 Rohres in einer der langsameren Oxidation des dünneren austenitischen Stahlrohres äquivalenten Zeit vor sich ging. Das ferritische Stahlrohr jedoch wurde wegen der geringeren Korrosionsbeständigkeit des Materials und der im Vergleich zum austenitischen Stahlrohr noch geringeren Wandabmessungen schneller umgesetzt. Neben der Oxidschichtbildung wurde auch die verschiedene sauerstoffreiche Phasen bildende Sauerstoff-Diffusion in die metallische Matrix messend verfolgt - auch im Blick auf deren Einfluß auf die mechanischen Eigenschaften und vor allem auf die Dimensionsänderungen.

1. Introduction

Isothermal and temperature-transient steam oxidation experiments are being performed at the Karlsruhe Nuclear Research Center as part of the Light Water Reactor (LWR) Safety Research Program of the Federal Republic of Germany. The experimental work contributes to worldwide research on the oxidation behavior of pressurized water reactor (PWR)-type Zircaloy-4 fuel rod cladding under loss-of-coolant and severe core damage conditions /1-3/.

After the Three Mile Island II reactor accident, the question frequently arose as to what the extent of oxidation of ferritic or austenitic steel cladding and in-core structural material under comparable accident conditions would have been. This question is of equal concern when candidates for the cladding material of an advanced type of PWR are considered /4/. Therefore, austenitic stainless steel cladding tubes have been examined in steam oxidation tests within the same time and temperature ranges as was done for Zircaloy-4 /5/. Equally, steam oxidation tests were performed with ferritic-martensitic steel cladding tubes /6/. This report summarizes and compares the results of the three above mentioned materials.

2. Experimental Procedure

The fuel cladding materials tested were

1. Standard-quality Zircaloy-4 as defined by the Kraftwerk Union (KWU) for PWR applications.
2. Austenitic stainless steel No. 1.4970 (DIN standard X10 NiCrMoTiB 15 15) as specified for liquid metal fast breeder reactor (SNR 300) applications.
3. Ferritic-martensitic steel No. 1.4914 (DIN standard X18 CrMoVNb 12 1) as applied in conventional and nuclear steam generation and being tested for fast and fusion reactor structural purposes.

The chemical analyses and tube dimensions are given in Table 1+2. Emphasis is put on the fact that different tube wall thicknesses (725 µm for Zircaloy-4, 500 µm for austenitic stainless steel No. 1.4970, 380 µm for ferritic-martensitic stainless steel No. 1.4914) were chosen for material testing. As specimens, 3-cm-long tube sections were inserted into an atmospheric pressure

laboratory steam loop (Fig. 1) and exposed on both sides to a flow of 0.1 g/s steam corresponding to a flow velocity of 1 m/s. The test temperatures ranged from 600 to 1300°C, and the duration from 1 to 6 h. The progress of metal oxidation was analyzed by gravimetry, metallography, and microanalytical methods (Fig. 2). The exposure was terminated when either the desired duration of exposure or - at the highest test temperature - total metal consumption was achieved.

The results are given in terms of:

- Weight gain in parabolic presentation,
- Arrhenius plots of reaction rate constants in comparable durations of exposure,
- Comparison of wall consumption,
- Various test results concerning
  - . wall penetration,
  - . wall consumption,
  - . hydrogen formation as reaction product,
  - . dimensional changes of the tube specimens.

3. Results

3.1 Steam Oxidation of Zircaloy-4 Tubing

The results of the Zircaloy-4 steam oxidation experiments performed between 600 and 1300°C for up to 6 h are presented in Fig. 3.

During an introductory phase of "normal" oxidation up to about 30 min an adherent oxide layer was formed. A cubic rate law is valid for 600-900°C, a parabolic one for 900-1300°C. The temperature dependence of K_p is expressed by the equation

$$K_p = 5.24 \cdot 10^9 \exp(-174.3/RT) \qquad [(mg/dm^2)^2/s]$$

The activation energy is given in kJ/mol.

After an extended exposure for up to several hours, three individual types of oxidation behavior were apparent:

- . From 600 to 800°C and at 1000°C, a transition from cubic or parabolic to a linear oxidation rate resulted from oxide scale cracking (the so-called breakaway effect).

- From 850 to 950°C, that is, in the two-phase (α + β)-Zr region, a change from cubic to parabolic oxidation was caused by a moderate breakaway effect. Presumably, it can be related to the changing mechanical properties in the Zircaloy two-phase region which allow partial relief of oxide growth stresses by plastic flow of the underlying bulk of the metal.
- At and above 1050°C, no change in rate law toward an accelerated oxidation was detected. The oxide scales remained adherent and protective during the whole exposure. Plastic flow of metal or oxide or both obviously could accomodate the tetragonal oxide growth stresses at the oxide/metal interface.

Slowing down of the reaction after 3 h at 1200°C and 1 h at 1300°C indicated that further oxidation (after having achieved total wall penetration by the ZrO_2/α-Zr(O)-double layers) would completely consume the α-Zr(O) metal core with the formation of zirconium dioxide (ZrO_2) as final product.

In two cases (800/900°C and 1000/1100°C) the final amount of oxygen taken up at the lower temperatures was larger than that at the higher temperatures. This effect was caused by oxide breakaway. As an example, Fig. 4 shows a sequence of cross sections of oxidized tube specimens. At 1000°C the specimens scale structure was affected by breakaway, resulting in faster oxidation than at 1100°C where, under otherwise equal conditions, integer oxide scales gave better protection. In the case of breakaway oxide scales, the α-Zr(O) sublayer was very thin or nearly missing. After having reached a critical scale thickness, periodical cracking of the oxide scale /7-9/ improves the oxygen transport to the ZrO_2/α-Zr(O) interface, causing a sudden rise of oxygen partial pressure. Thus, further ZrO_2 formation proceeds at about linear rate whereas the oxygen diffusion into the metal, is determined by the ZrO_2 dissociation pressure at the interface. Fig. 5 shows the state of oxidation achieved after six hours exposures at 1000-1300°C.

Dimensional changes of the outer and inner diameter of the oxidized tubing were measured by a slide gage and metallography. In the case of double-sided oxidation at 1200 and 1300°C, the outer diameter of Zircaloy-4 tubing expanded by up to 12%, and the inner diameter by up to 8%. The corresponding gain in wall thickness was about 30% to 60%.

3.2 Steam Oxidation of Austenitic Stainless Steel No. 1.4970 Tubing

The steam oxidation kinetics of the austenitic stainless steel No. 1.4970 tubing have been investigated at the same time and temperature ranges as was done for Zircaloy-4 tubing. The extent of oxidation was measured by gravimetric and metallographic means since no spalling occurred under extended exposures. Oxygen uptake is plotted versus square root of time in Fig. 6. In principle, the oxidation kinetics from 600 to 1300°C can be expressed as parabolic functions. However, at 1250 and 1300°C and after 200 and 100 min, respectively, the reaction rate slowed down, finally approaching zero after the tubing was nearly completely oxidized. At lower temperatures the reaction rate law remained parabolic throughout the exposure time. An Arrhenius plot of the parabolic rate constant K_p signalized no change in activation energy over the chosen temperature range of testing, which meant that the rate determining diffusion process remained unchanged. The temperature dependence of K_p can be expressed by the equation

$$K_p = 2.80 \cdot 10^{11} \exp(-227/RT) \qquad [(mg/dm^2)^2/s]$$

in which the activation energy is given in kJ/mol. Fig. 7 shows the state of oxidation achieved after a six hours exposure at 1000-1300°C.

As reaction products (Fig. 8), an external scale of wüstite and magnetite in addition to an inner one of iron-nickel-chromium spinel were formed. A remarkable extent of swelling accompanied progressing oxidation. The dimensional changes of the tubing (Fig. 9) were measured after exposure at 1200, 1250, and 1300°C and found to be linear functions of weight increase (Fig. 10). The increase in outer diameter was symmetrical to the decrease of the inner diameter, both about 10%. The corresponding gain in wall thickness was about 120%.

3.3 Steam Oxidation of Ferritic-Martensitic Steel No. 1.4914 Tubing

The steam oxidation kinetics of the ferritic-martensitic stainless steel No. 1.4914 tubing have been investigated /6/ at the same time and upper temperature ranges as was done for Zircaloy-4 and CrNi stainless steel No. 1.4970.

Since this material did not show spalling in the oxidized condition within the temperature range 900-1300°C the measured weight gain could be directly related to the oxygen uptake. In Fig. 11 the oxygen uptake is plotted versus the square root of time. In principle, the oxidation kinetics from 900 to 1300°C can be given as parabolic functions. The fact that after 10 min, 1300°C; 20 min, 1200°C; 30 min, 1100°C; and 60 min, 1000°C the reaction slowed down considerably indicated that after certain degree of wall penetration was achieved the approximation to the stated total oxidation went on asymptotically. Since there was no change in activation energy, the respective rate constants could be calculated on the basis of the parabolic functions being represented as straight lines up to the exposure times at temperature, as indicated above. The temperature dependence of K_p can be expressed by the equation

$$K_p = 3.51 \cdot 10^{11} \exp(-203.2/RT) \; [(mg/dm^2)^2/s]$$

in which the activation energy is given in kJ/mol.
Fig. 12 gives an example of progress of wall oxidation at 1100°C while Fig. 13 shows the state of oxidation achieved at 1300°C after 2.5-20 min exposure time. As reaction products /10/ an external scale of magnetite Fe_3O_4(+FeO) and wüstite FeO(+Fe_3O_4) and an inner scale of the type iron-chromium spinel (Fe Cr_2O_4) could be detected. The outer scale layer (Fig. 14) is compact and built of large crystals with well defined crystallographic planes. It is metallic grey but some still brighter regions can be also distinguished on metallographic cross-sections. On certain specimens these brighter regions form a separate outer-most scale layer. X-ray analysis has shown that the outer scale is composed of wüstite, FeO, with magnetite, Fe_3O_4, dispersions. The latter are present in greater amounts near the scale/gas interface than in the vinicity of the inner scale layer. At 1000-1300°C the outer scale is built of two sublayers separated by columnar oxide grains of variable orientation. With increasing temperature the inner sublayer becomes porous, the dimensions and amount of pores being a function of temperature, their shape being mostly oval. Observations with the aid of the scanning microscope have proved that these pores are generally situated along the grain boundaries. The inner scale layer (Fig. 14) consisting mostly of a mixture of wüstite, FeO, and spinel $FeCr_2O_4$, is not uniform and homogeneous. There are some particular porous regions within this layer, characteristic by irregular and joined-together oxide crystals of random orientation. It has been found that

these regions are rich in chromium normally bound to the iron-chromium spinel. The chemical composition of the spinel is difficult to determine since it is dispersed within the FeO matrix. The remaining part of the inner scale layer is compact. This part is also characterised by micropores and holes. EDX analysis has shown that this part of the scale exhibits a significant concentration of iron and a small amount of chromium.

In the inner scale layer, on all the specimens oxidized at 900-1300°C, there are metallic inclusions (Fig. 15), the shape, amount, dimensions, and chemical composition of which depend on the distance from the metallic core and on temperature. In the region adjacent to the metallic core these inclusions are irregular in shape and their diameter reach 6 µm. The inclusions become enriched in nickel at the cost of chromium and iron, the concentrations of which decrease. In the outer-most part of the inner scale layer the concentration of nickel is about twenty times as high as that near the metallic core.

The metallic core (Fig. 12-15) has shown in the chemical analysis a certain chromium depletion adjacent to the scale as a consequence of the oxidation process. Platinum markers (Fig. 15), attached to the metallic surface before oxidation,were found after the reaction to be located at the boundary between the outer and the inner scale. This indicated that the formation of the outer layer took place due to outward diffusion of iron and the inner layer as a result of inward diffusion of oxygen.

4. Comparison of Materials Behavior

4.1 Procedures of Evaluation

In general, the appropriate way of evaluating the oxidation behavior of different materials is to check whether it can be described by an equal or similar rate law and, if so, to compare their rate constants as functions of temperature (Fig. 16).

In our practice this kind of comparison cannot be done without major difficulties because the limited tube material available for oxidation causes,

at the very high temperatures, deviations from straight parabolic behavior when total metal consumption is approached ; and in addition, it was shown that Zircaloy-4 oxidation is governed by various rate laws in the initial oxidation period and changes in rate law during extended exposure.

Therefore, a comparison of materials behavior as function of time and temperature has to be based on direct but less-precise calculations of reacted metal and wall consumption (derived from oxygen uptake) and also on wall penetration measurements from metallography.

The weight of oxygen consumed during the oxidation reaction was transformed into weight of reacted metal by multiplying by a factor based on the metal content of the corresponding stoichiometric metal oxides. This calculation of reacted metal however neglects the distribution of oxygen in the metallic phase. For Zircaloy-4, the calculations are based on the formation of fully stoichiometric ZrO_2. The corresponding factor by which weight gain had to be multiplied to obtain reacted metal is 2.85.

The gain in weight of the austenitic and ferritic steels was transformed into weight of reacted metal by multiplying by the factor 2.56 (austenite) or 2.40 (ferrite), which are average factors based on the formation of iron oxide (Fe_2O_3), chromium oxide (Cr_2O_3) and nickel oxide (NiO) as final stoichiometric oxidation products. By relating the amount of reacted metal to the initial specimen weight, the percentages of reacted metal or consumed wall thickness could be calculated.

4.2 Reacted Metal/Consumed Wall Thickness

Figures 17 + 18 summarize for all materials the calculated percentages of tube wall consumed as function of time. In all cases, 100% consumption was never found because of the existing stoichiometric uncertainties and the possibility that total stoichiometric composition was never fully achieved. Naturally, the actual curves of consumption kinetics correspond to those of weight gain measurements.

The direct comparison of the materials behavior (Table 3) could be performed on the basis of percentage of wall consumption. Thus it became obvious that, although the Zircaloy-4 oxidation proceeded significantly faster than that

of the austenitic stainless steel, the differing tube wall dimensions caused the proportions of consumed material (under equal exposure times) to be similar at the lower temperatures and almost equal at the higher temperatures. Because of its thin wall thickness, the ferritic steel tubing became oxidized much faster. Another way of comparing the materials oxidation behavior is to calculate fictitious 6 h-exposures over the whole temperature range by assuming that the consumption of unlimited wall thicknesses takes place by oxidation reactions, which are governed by constant parabolic rate laws (as elaborated from the true linear part of the functions of mass increase versus square root of time and given for all three materials). The result is shown in Fig. 19 which proves the ranking position of Zircaloy-4 is between the steels of which the ferritic-martensitic Cr steel is the less resistant and the austenitic NiCr steel is the most resistant one. Certain unexpected high values of Zircaloy-4 wall consumption are due to the breakaway effect which was at critical temperatures taken into account by linear extrapolation. The 600-800°C results of No. 1.4914 steel originate from sheet specimen testing under equal conditions where no spalling occurred.

4.3 Wall Penetration

Progress of Zircaloy-4 and stainless steels oxidation can also be described by metallographic analyses, by measuring the extent of wall penetration caused by oxide scale and sublayer formation. Oxidation of Zircaloy-4 took place by formation of the already mentioned ZrO_2/α-Zr(O) double layers. The stainless steels were oxidized by formation of outer iron-rich and inner chromium-rich scale layers, the latter often containing a large number of small metallic particles. The state of oxidation was given in Figs. 4, 5, 7, 12 for the materials. When equal notice was taken of other micrographs of intermediate states of oxidation, it became obvious that wall penetration by formation of uniform oxide scales and other oxygen-containing phases always proceeded faster than calculated wall consumption. Practically independent of reaction temperature, complete Zircaloy-4 tube wall penetration occurred after an uptake of more than 50% of the oxygen needed for calculated total metal consumption, while in case of the stainless steels more than 80% was required.

4.4 Combined Effects

A comparison of the dimensional changes of highly oxidized Zircaloy-4 and the stainless steels (6 h, 1200 to 1300°C) is given in Table 3. All materials showed an increase in the outer diameter of 10% to 15%, but the inner diameter expanded in the case of Zircaloy-4 and became smaller for the stainless steel tubings: No influence on fuel rod coolability under accident conditions can be derived from these results.

Hydrogen production took place according to the measured oxidation kinetics. When a protective, dense and compact oxide scale is formed on Zircaloy-4, only a small fraction of hydrogen is dissolved in the zirconium matrix. In case of non-protective breakaway oxide scale growth more hydrogen is taken up /11/, but is re-evolved progressively when total oxidation takes place.

The solubility in the stainless steel matrices is so small that hydrogen up-take is not considered here, all hydrogen will be liberated.

For calculation of hydrogen generation stoichiometric factors are used, based on an idealized composition of the reaction products like ZrO_2 and FeO, Fe_3O_4, Fe_2O_3, Cr_2O_3, NiO. For all materials the substoichiometric oxide composition remains an uncertainty of calculation. Since total oxidation remains about 5-10% below the theoretical value of oxygen uptake to form the above mentioned oxides, the same can be assumed for the hydrogen production.

5. Conclusions

The double-sided steam oxidation of Zircaloy-4 and two stainless steels, the austenitic CrNi-steel No. 1.4970 and the ferritic-martensitic Cr-steel No.1.4914 under off-normal and accident LWR-conditions, i.e. during short durations and at temperatures far above the limit of application for engineering purposes, could be described as follows:

- Oxygen up-take can be approximated by parabolic rate equations over wide ranges of time and temperature. If some deviations - due to breakaway of oxide scales and beginning wall consumption - are omitted, an Arrhenius plot of the parabolic rate constants allows a time-

- limited comparison of the oxidation rates of the three materials and a calculation of the respective activation energies.

. The relatively uniform oxidation behavior of the materials can be explained by the formation of initially adherent, dense and protective oxide scales. These scales, however, can be matter of transformation to mechanically defect oxide structures (after periods related closely to scale growth of critical temperature dependent oxide thickness) which then start to grow at an accelerated rate of metal consumption.

. Considerable changes of tube dimensions due to creep under oxide growth stresses could be measured. Their importance has to be estimated on the basis of special core design features and the high temperature properties under oxidizing conditions.

. The oxidation products are different in respect to their fusion temperatures: while ZrO_2 remains solid up to 2700°C, the iron, chromium and nickel oxides are melting already below 1500°C, a behavior which is certainly of relevance to the accident considerations and the choice between standard and advanced LWR core materials.

6. Acknowledgements

The authors gratefully acknowledge the experimental contribution of H. v. Berg and the metallographic work of Mrs. B. Bennek-Kammerichs. The investigation was performed as part of the Nuclear Safety Project, subtask material selection for an Advanced Pressurized Water Reactor.

7. References

/1/ Leistikow, S., Schanz, G., and von Berg, H., "Kinetik und Morphologie der isothermen Dampf-Oxidation von Zircaloy 4 bei 700-1300°C", KfK 2587, 1978

/2/ Leistikow, S., Schanz, G., and von Berg, H., "Untersuchungen zur temperatur-transienten Dampfoxidation von Zircaloy 4-Hüllrohrmaterial unter hypothetischen DWR-Kühlmittelverlust-Störfallbedingungen", KfK 2810, 1979

/3/ Leistikow, S., Schanz, G., von Berg, H., and Aly, A.E. in Proceedings, OECD-NEA-CSNI/IAEA Specialists Meeting on Water Reactor Fuel Safety and Fission Product Release in Off-Normal and Accident Conditions, Risø, Denmark, 16-20 May 1983, IAEA-Summary Report IWGFPT/16 (1983) pp. 188-199

/4/ Kuczera, B., and Küsters, H., Kernforschungszentrum Karlsruhe-Nachrichten, No. 14, 1982, p. 34

/5/ Leistikow, S., "Comparison of High-Temperature Steam Oxidation Kinetics Under LWR Accident Conditions: Zircaloy-4 Versus Austenitic Stainless Steel No. 1.4970", Zirconium in the Nuclear Industry: Sixth International Symposium, ASTM STP 824, D.G. Franklin and R.B. Adamson, Eds., American Society for Testing and Materials, 1984, pp. 763-779

/6/ Zurek, Z., "Isothermal Steam Oxidation of the Ferritic 11% Cr Steel (DIN No. 1.4914) at 900 to 1300°C", KfK 3436, 1982

/7/ Bennek-Kammerichs, B., Franz, J., Leistikow, S., and Schanz, G., "Untersuchungen über das Erscheinungsbild und die kinetischen Folgen gestörter Deckschicht-Bildung bei der Zircaloy-4/Wasserdampf-Hochtemperatur-Oxidation", KfK 3052, 1980

/8/ Schanz, G., and Leistikow, S. in Proceedings, American Nuclear Society/European Nuclear Society Topical Meeting on Reactor Safety Aspects of Fuel Behavior, Sun Valley, Idaho, Vol. 2. 2-6 Aug. 1981, p. 342

/9/ Schanz, G., and Leistikow S. in Proceedings, 8th International Congress on Metallic Corrosion, Mainz, FR Germany, Vol. 2. 6-11 Sept. 1981, p. 1712

/10/ Zurek, Z., Leistikow, S., and Schanz, G., "Morphology and Chemical Composition of Scales Formed on Fe-11Cr Steel Oxidized in Steam at 900-1300^{o}C", Proceedings Seventh European Congress of Corrosion, Nice, France, 19-21 Nov. 1985 (to be published)

/11/ Schanz, G., and Leistikow, S., "Zur konkurrierenden Sauerstoff- und Wasserstoffaufnahme des Zircaloy-4 bei hohen Temperaturen", in Proceedings DGM/GDMB Meeting "Gase in Metallen", D. Hirschfeld Edt., Deutsche Gesellschaft für Metallkunde e.V., Darmstadt, Fed. Rep. Germany, 28-30 March, 1984, pp. 413-426

Table 1: Chemical Analyses of Tube and Sheet Materials (wt%)

Material	Shape	Sn	Fe	Cr	O	Zr
Zircaloy-4	Tube	1.35-1.47	0.19-0.21	0.09-0.10	0.12	98.1-98.25

		C	Si	Mn	Cr	Ni	Mo	V	Ti
CrNi-Steel	Tube	0.09	0.4	1.60	14.9	15.0	1.19	0.05	0.43
(Mater.No.1.4970)		Ta	B	Co	Ca	Fe			
		0.02	0.005	0.02	0.005	66.3			

		C	Si	Mn	P	S	Cr	Ni	Mo
Cr-Steel	Tube	0.21	0.34	0.3	0.001	0.006	11.5	0.77	0.60
(Mater.No.1.4914)	Sheet	0.17	0.34	0.54	0.005	0.005	10.6	0.82	0.49
		V	Nb	Ti	Co	Cu	Fe		
	Tube	0.31	0.24	0.006	0.006	0.024	85.5		
	Sheet	-	0.19	-	0.015	-	86.8		

Table 2: Dimensions of Tube and Sheet Materials (mm)

	Tube			Sheet
	OD	ID	Wall	Thickness
Zircaloy-4	10.75	9.30	0.725	-
Austen. CrNi-Steel Mater.No.1.4970	7.6	6.6	0.5	-
Ferr.-martens. Steel Mater.No.1.4914	6.0	5.24	0.38	1

Table 3: Dimensional Changes of Tube Materials after Extended Steam Exposure (6 h, 1200-1300°C) (%)

	OD	ID	Wall
Zircaloy-4	+ 12	+ 8	+ (30-60)
Austenitic CrNi-Steel Mater. No. 1.4970	+ 10	- 10	+ 120
Ferritic-Martensitic Cr-Steel Mater. No. 1.4914	+(12-15)	-(12-15)	+(150-190)

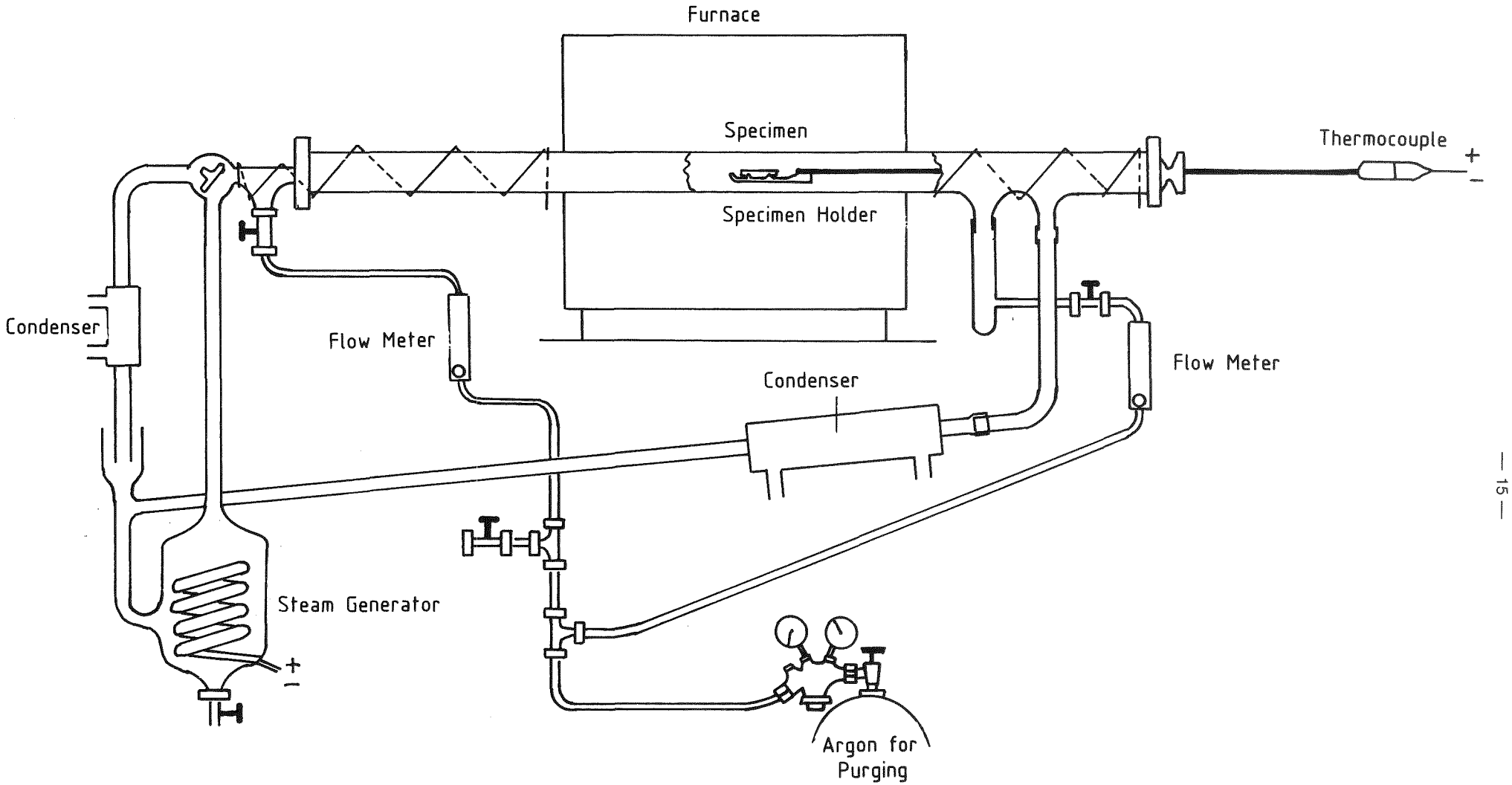

Fig. 1 **Test Facility for Steam High Temperature Oxidation Experiments**

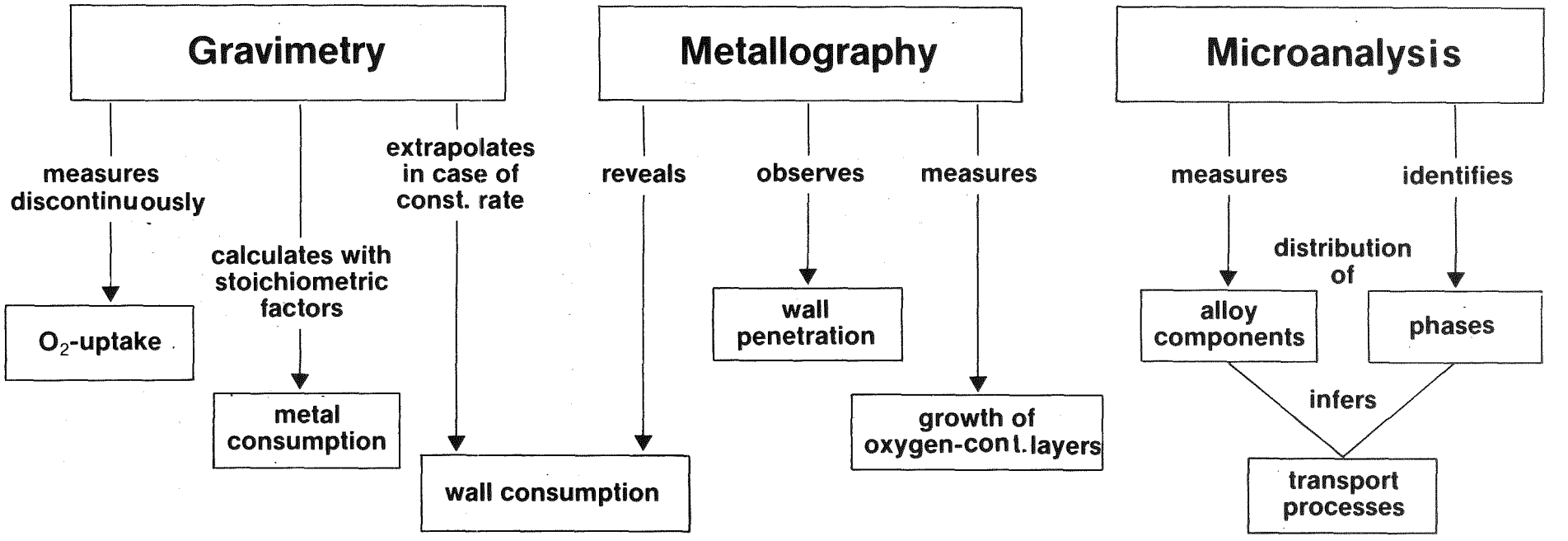

Fig. 2

Scheme of Methods and Their Capabilities to Evaluate HT Oxidation Investigations

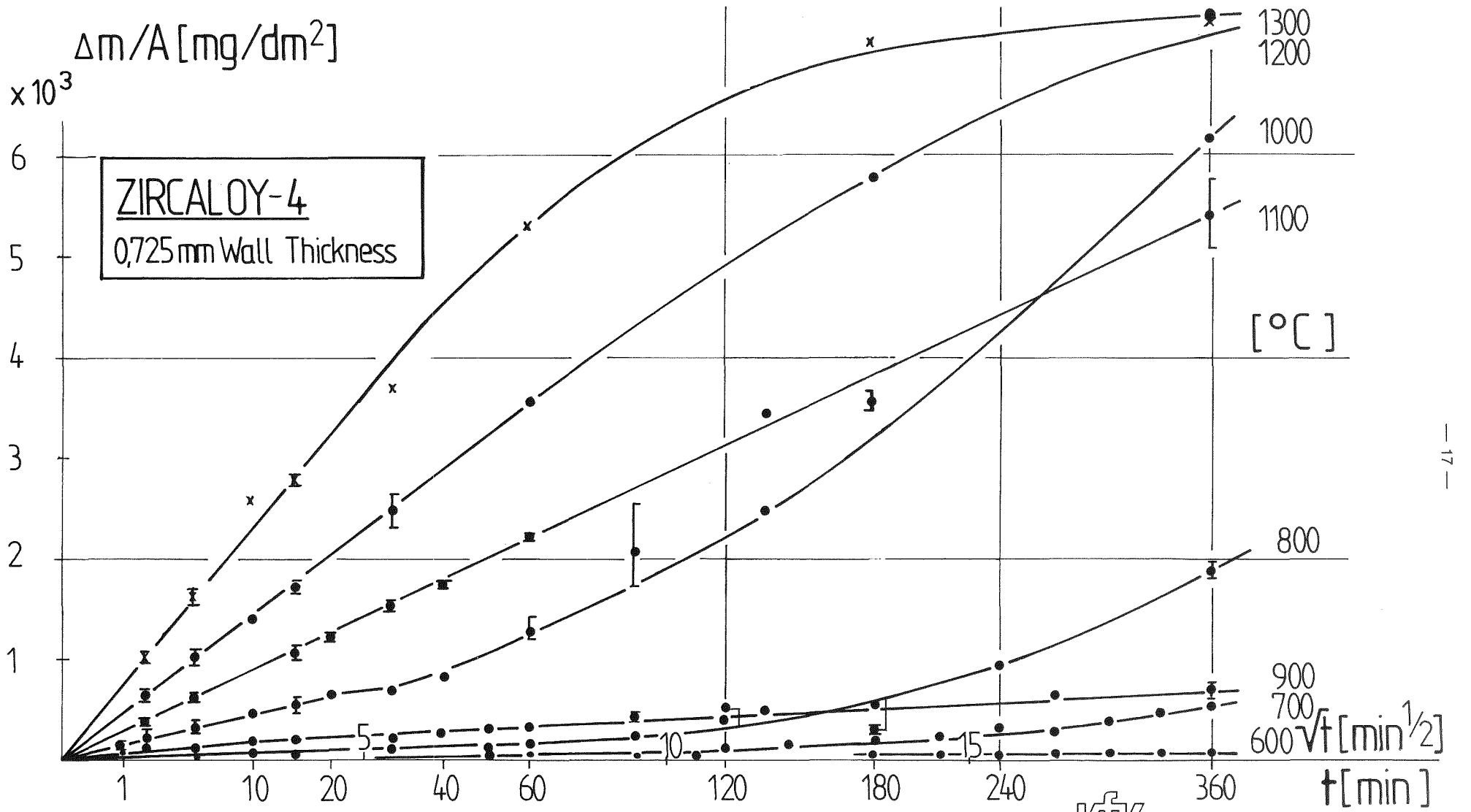

Fig. 3

363 KfK IMF/II-PNS

Zircaloy-4 Cladding Tube Steam Oxidation ; Weight Gain versus Time of Exposure

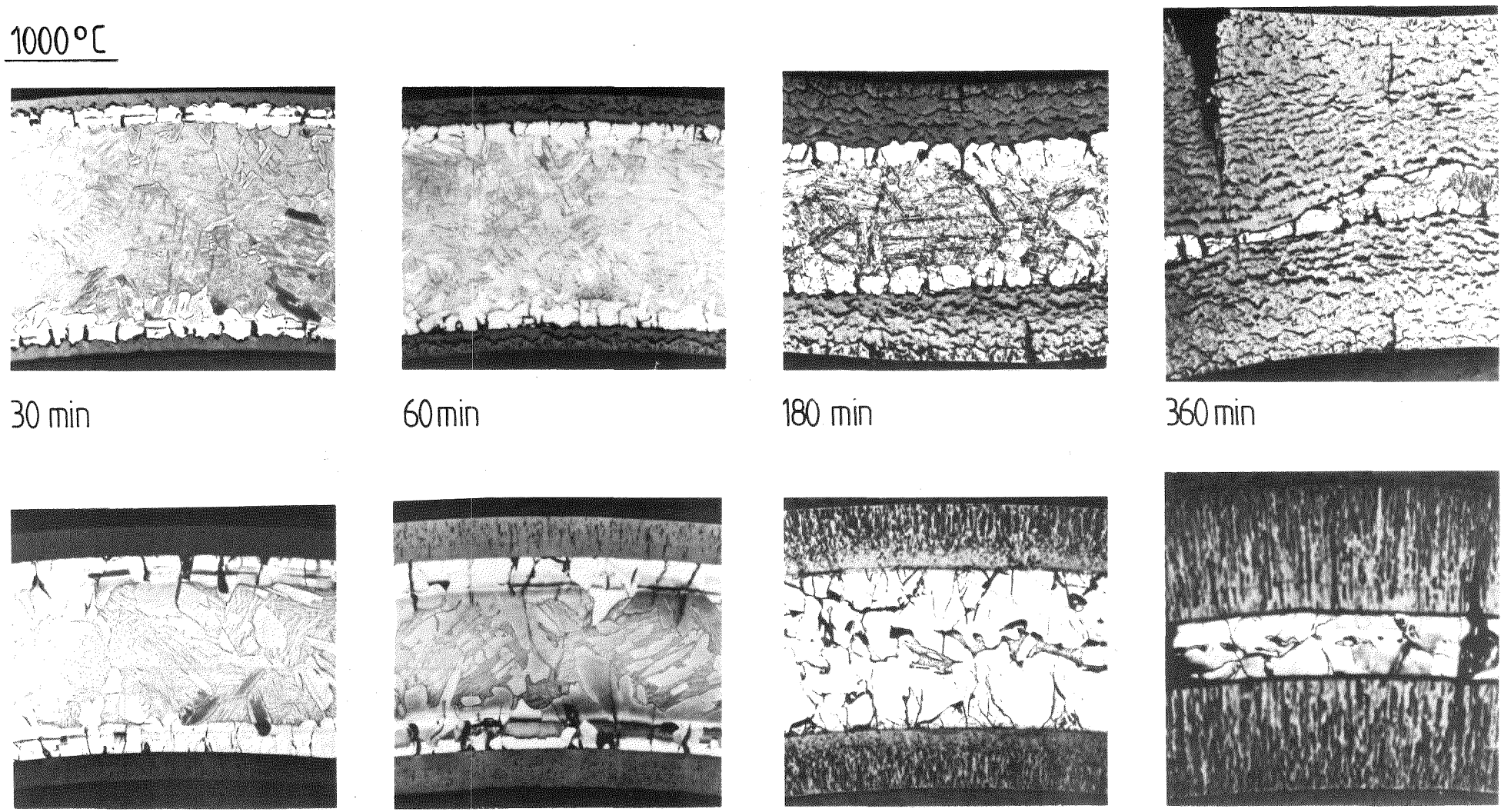

Fig. 4
Isothermal Zircaloy -4 / Steam Oxidation with Respect to the Typical Breakaway (1000°C) and Non-Breakaway (1100°C) Oxide Morphology

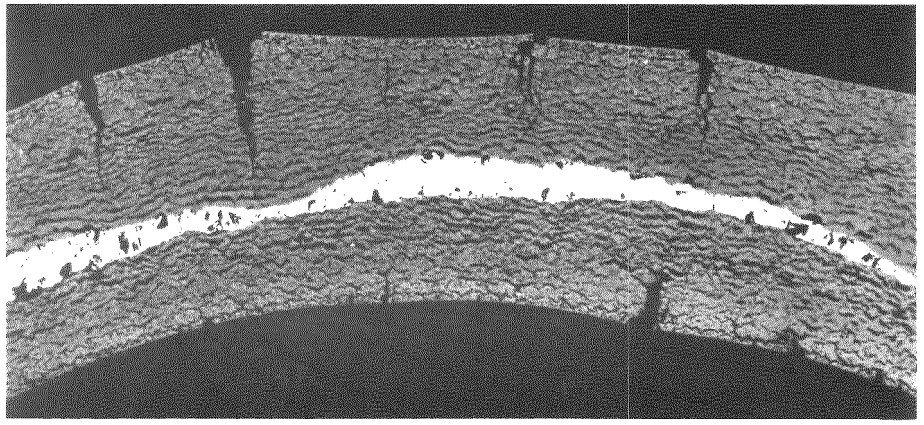

1000 °C

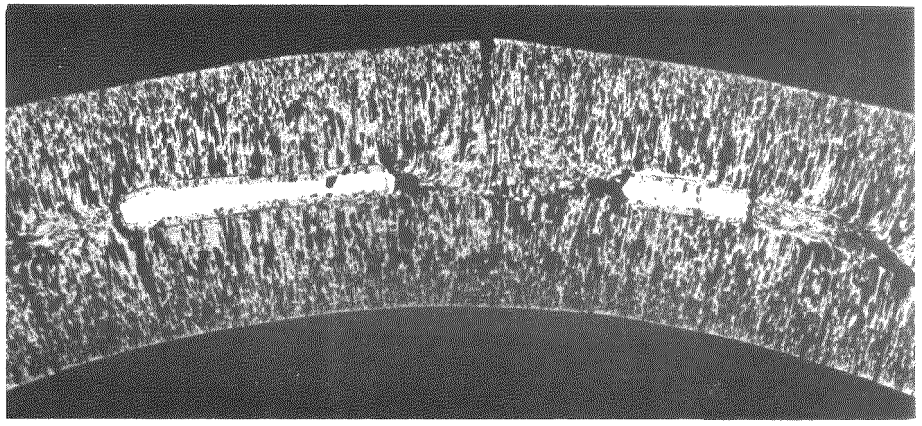

1200 °C

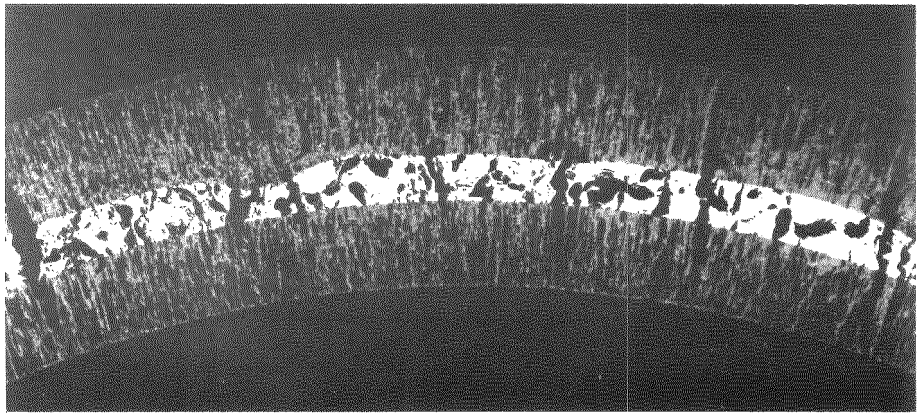

1100 °C

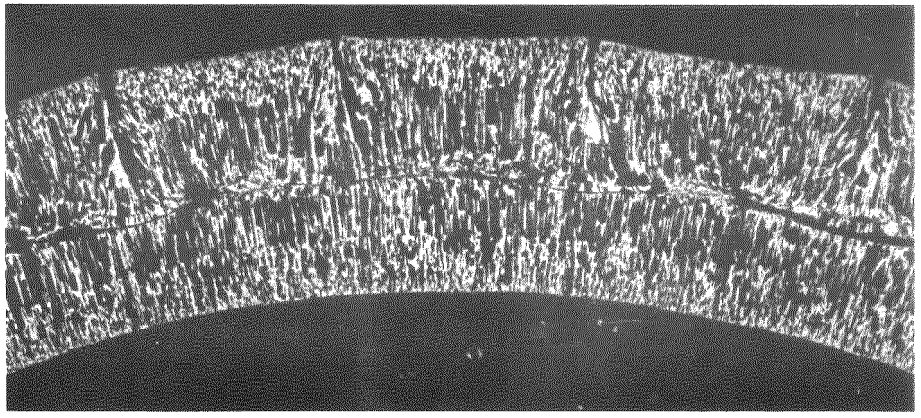

1300 °C

⟷ 200 µm

Fig. 5

Steam Oxidation of Zircaloy-4 under LWR-Accident Conditions (6 h, 1 bar)

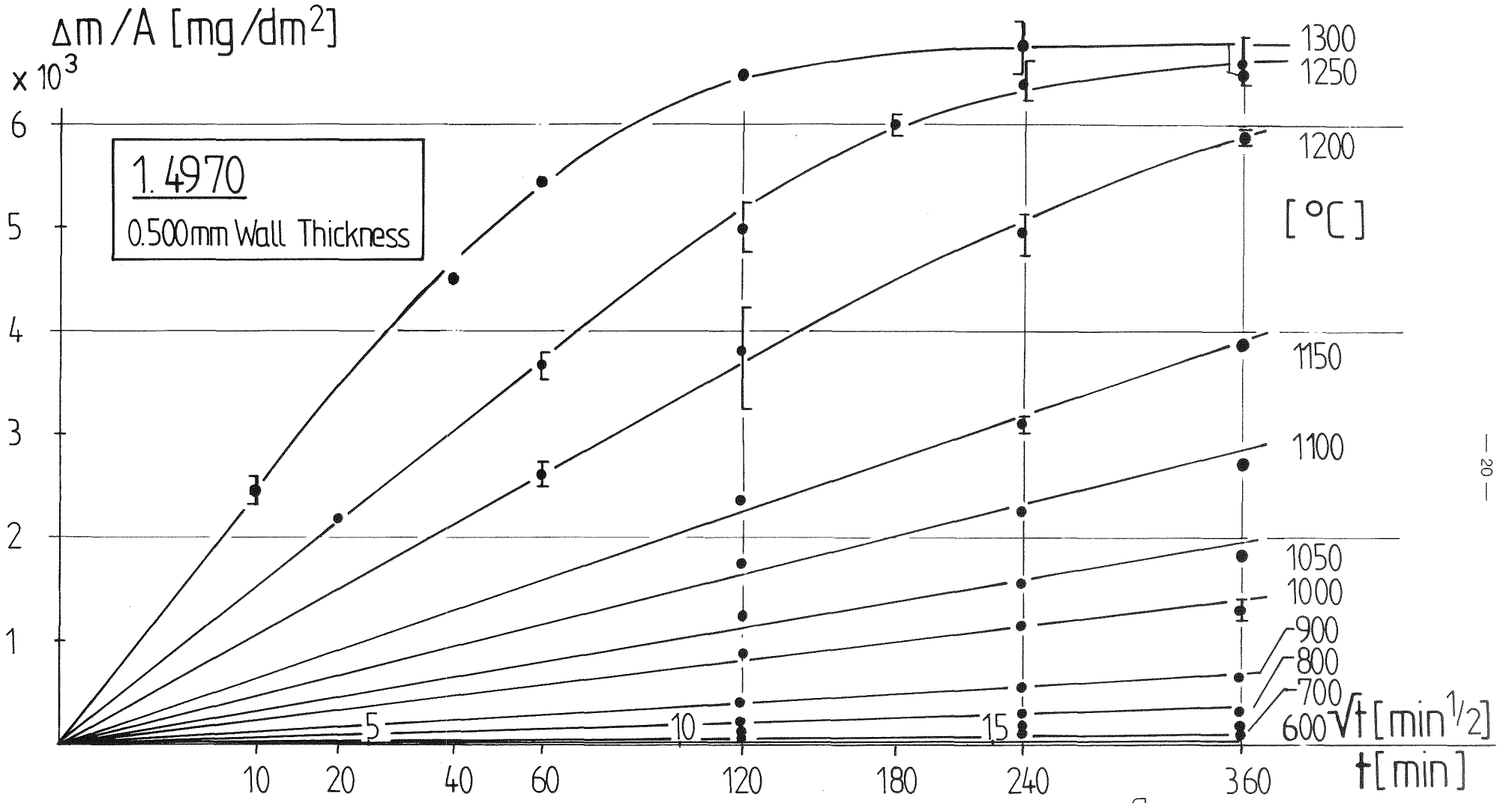

Fig. 6

364 KfK IMF/II-PNS

Austenitic Stainless Steel No. 1.4970 Cladding Tube Steam Oxidation
Weight Gain versus Time of Exposure

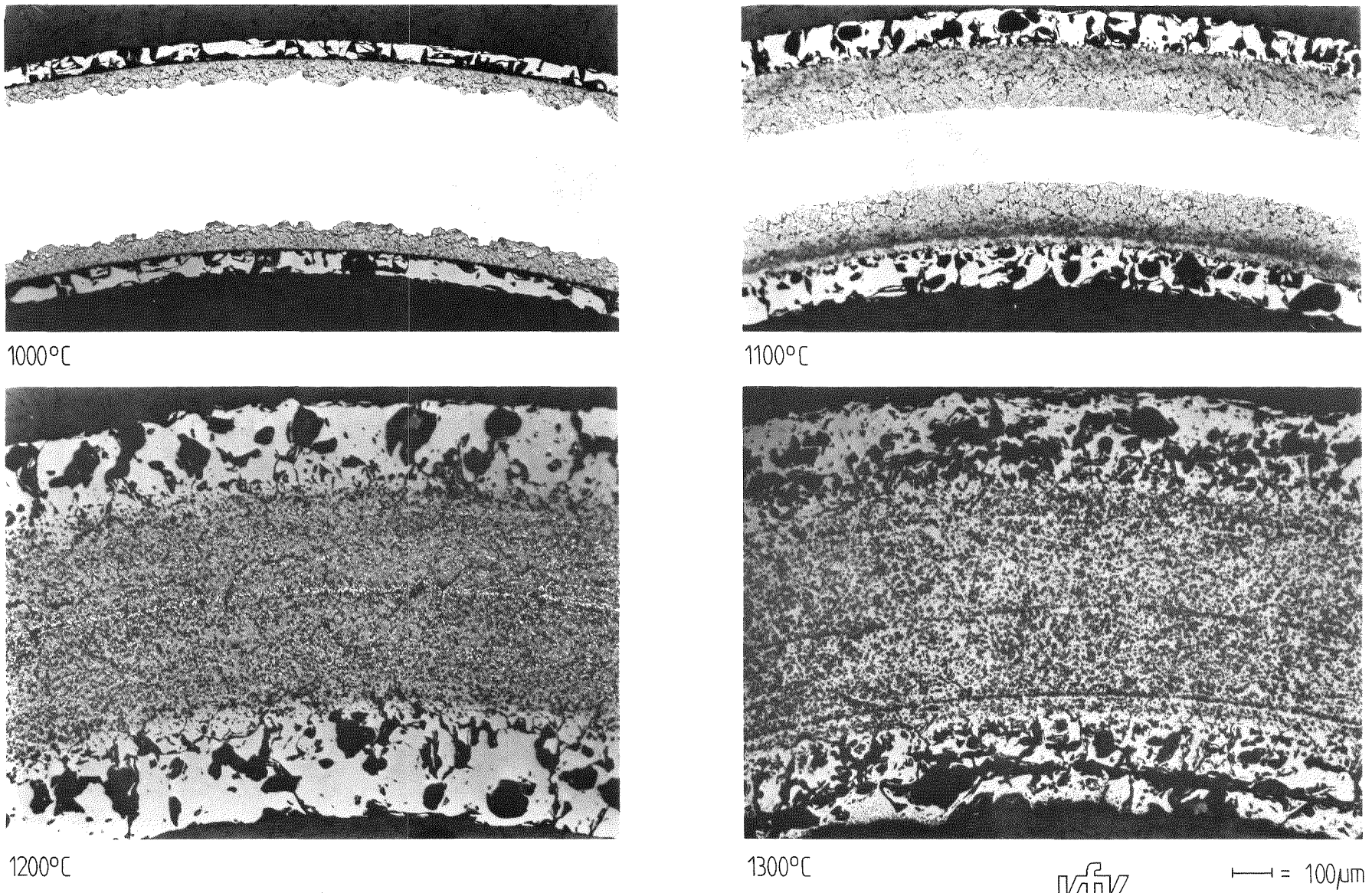

Fig. 7

HT-Steam Oxidation of Material No. 1.4970 Under FDWR-Accidental Conditions (6 h, 1 bar)

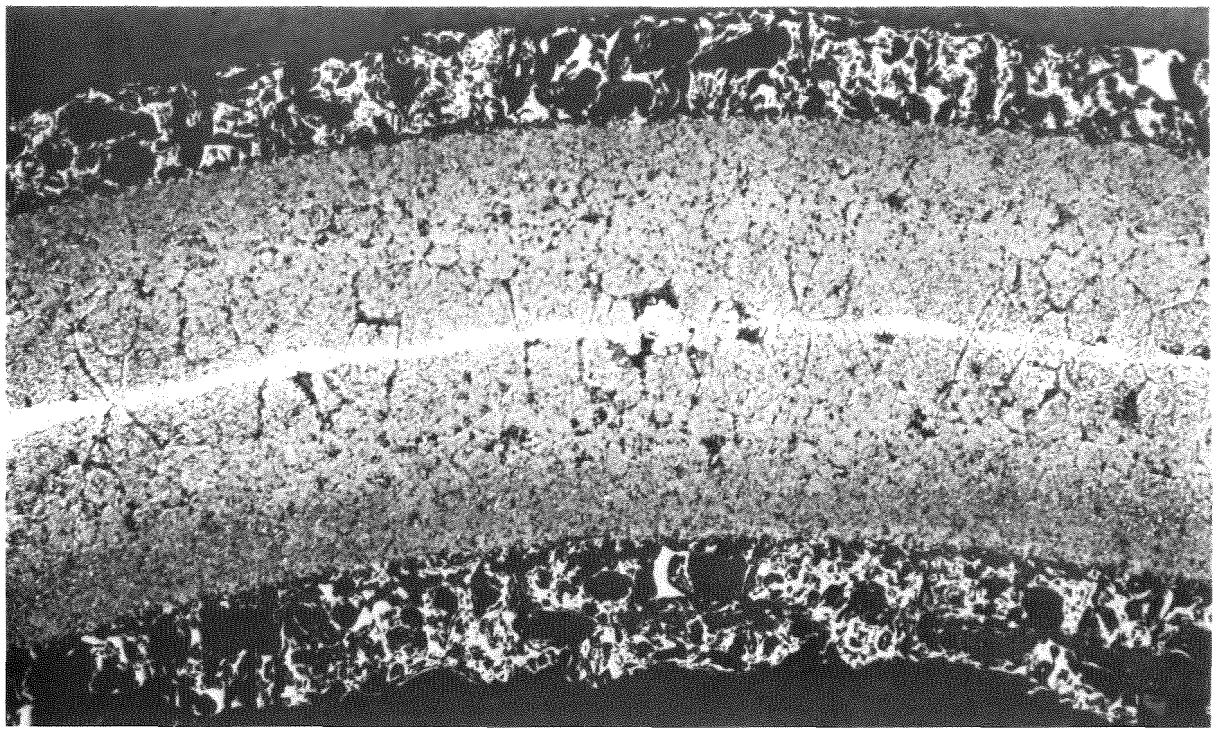

A)

⟷ 100 µm

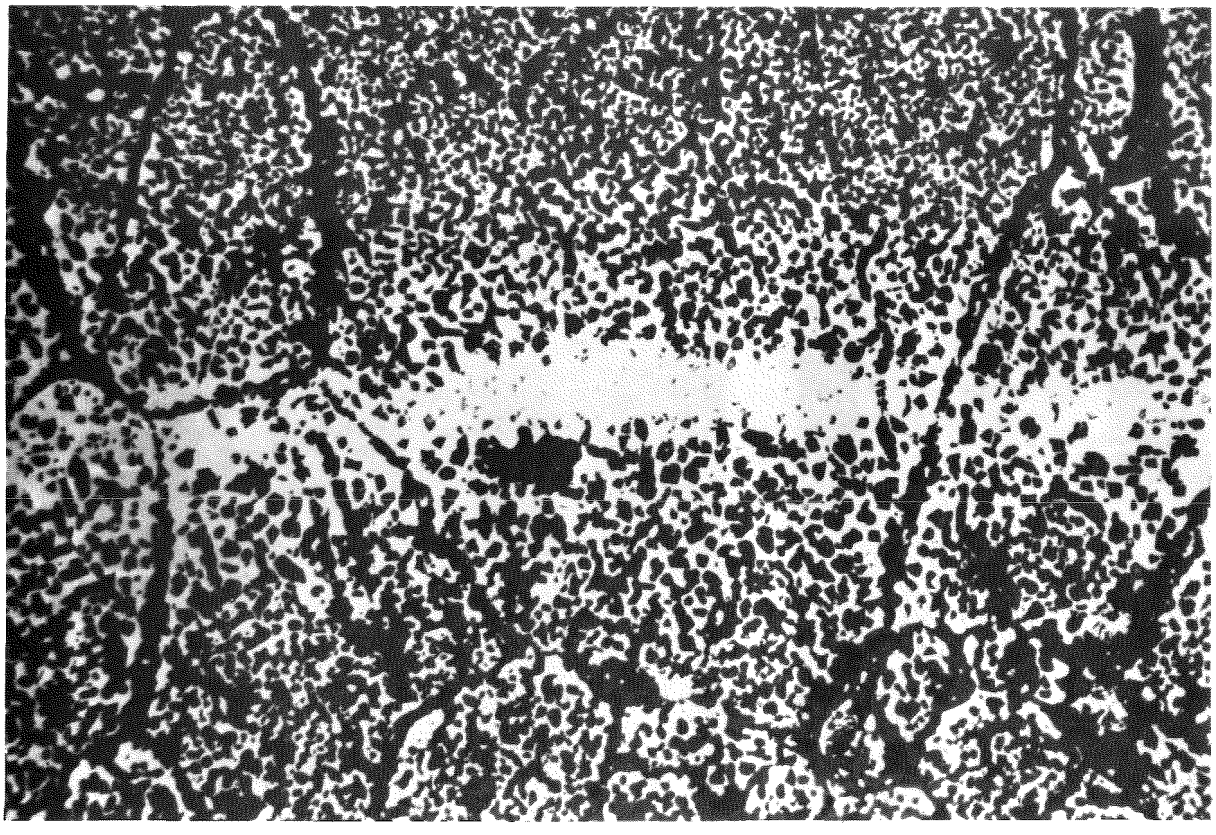

B)

⟷ 20 µm

Fig. 8

Steam Oxidation of Material No. 1.4970 under LWR-Accident Conditions (4 h, 1200°C)
A) total wall B) middle of wall

1300 °C

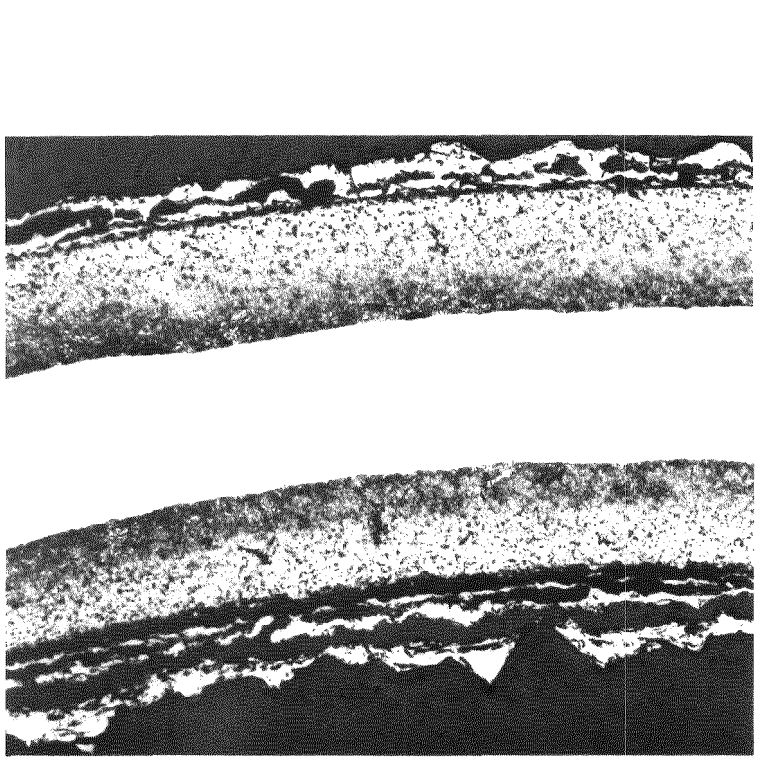

10 min

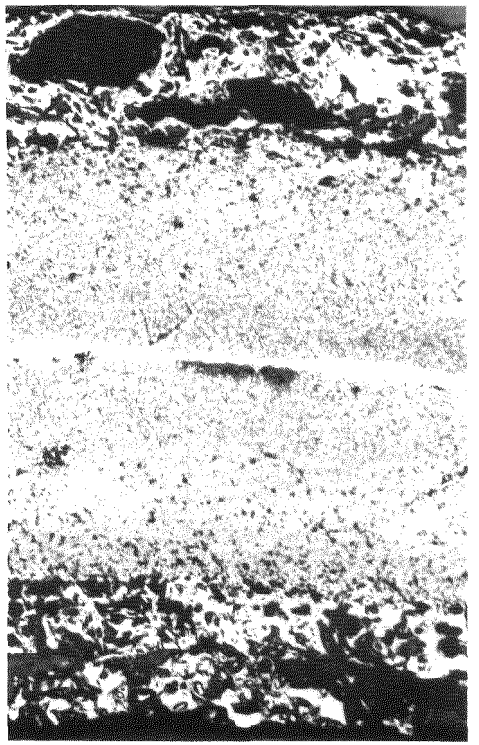

60 min

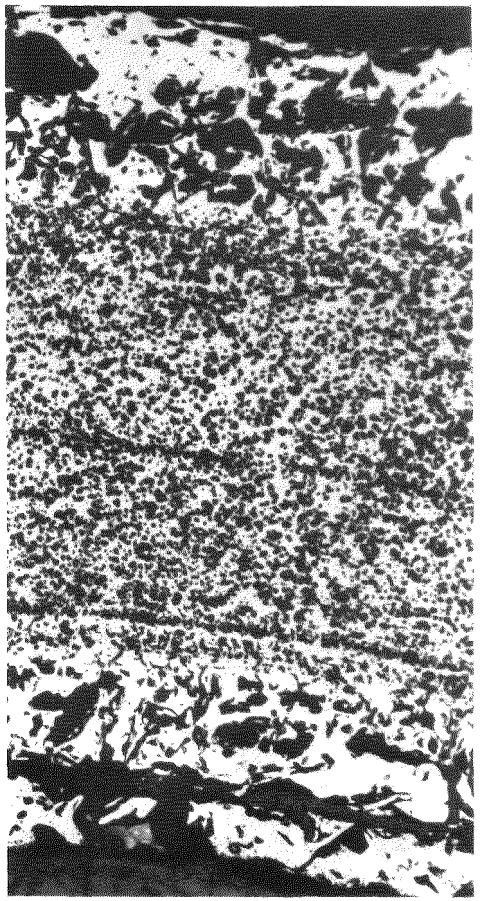

360 min

100 µm

Fig. 9

Austenitic Stainless Steel No. 1.4970 / Steam Oxidation
Growth of Wall Thickness until Total Metal Consumption

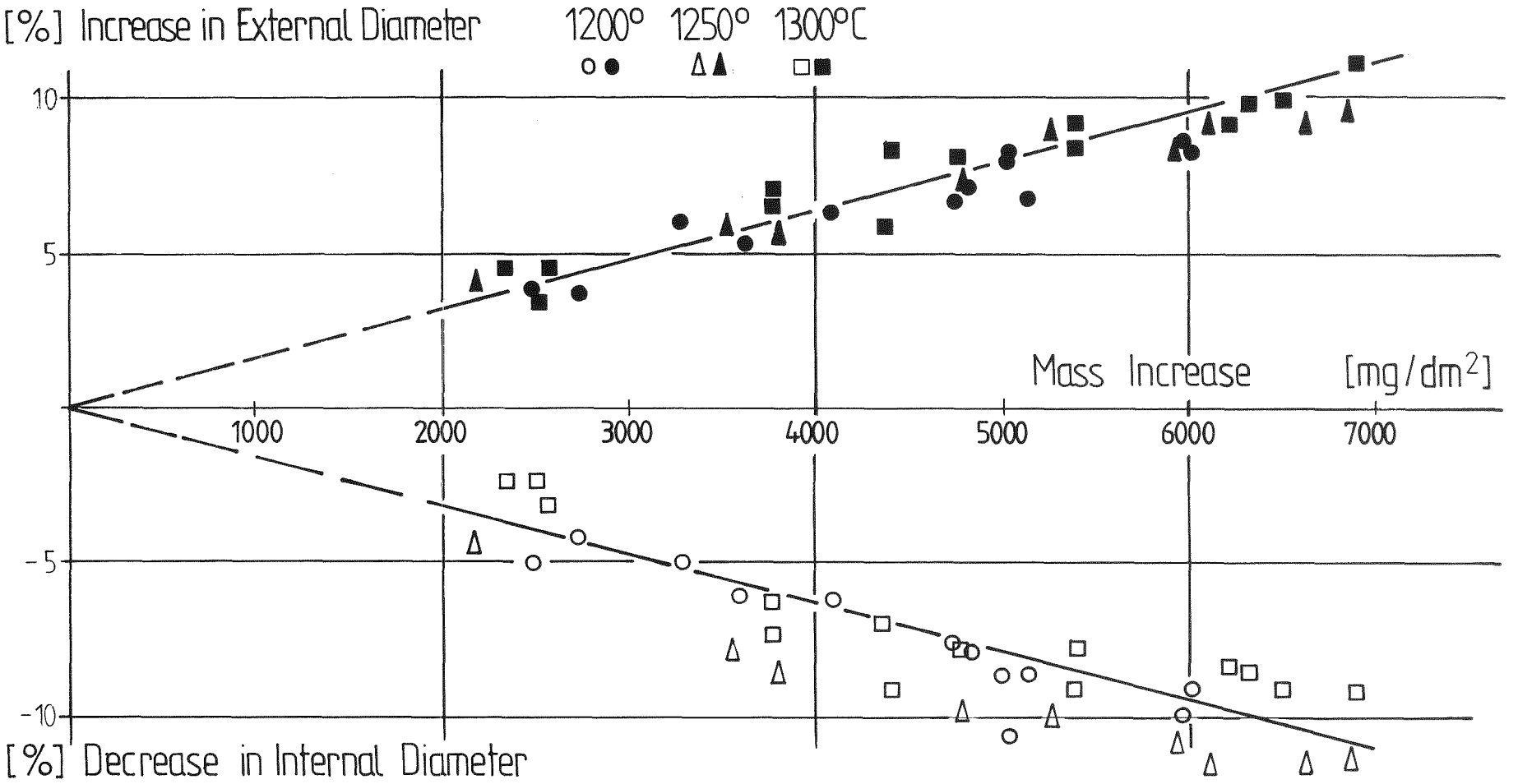

KfK

Fig. 10

Austenitic Stainless Steel No. 1.4970 / Steam Oxidation
Dimensional Changes versus Mass Increase of Tubing (7,6 mm OD / 0,5 mm Wall Thickness)

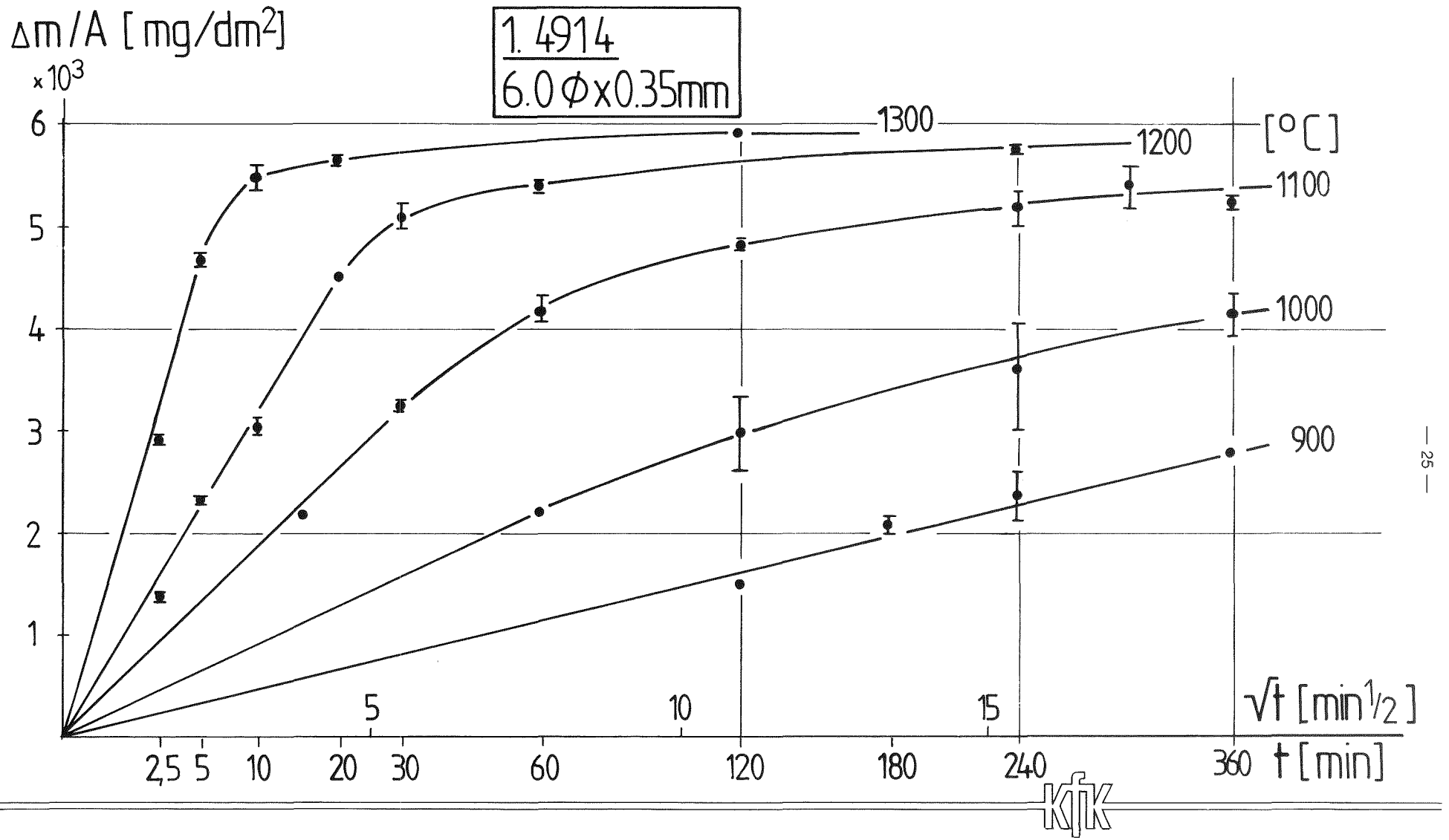

Fig. 11 Steam Oxidation of Material No. 1.4914 under LWR-Accident Conditions
Mass Increase of Tube Material. (6 h, 900-1300°C)

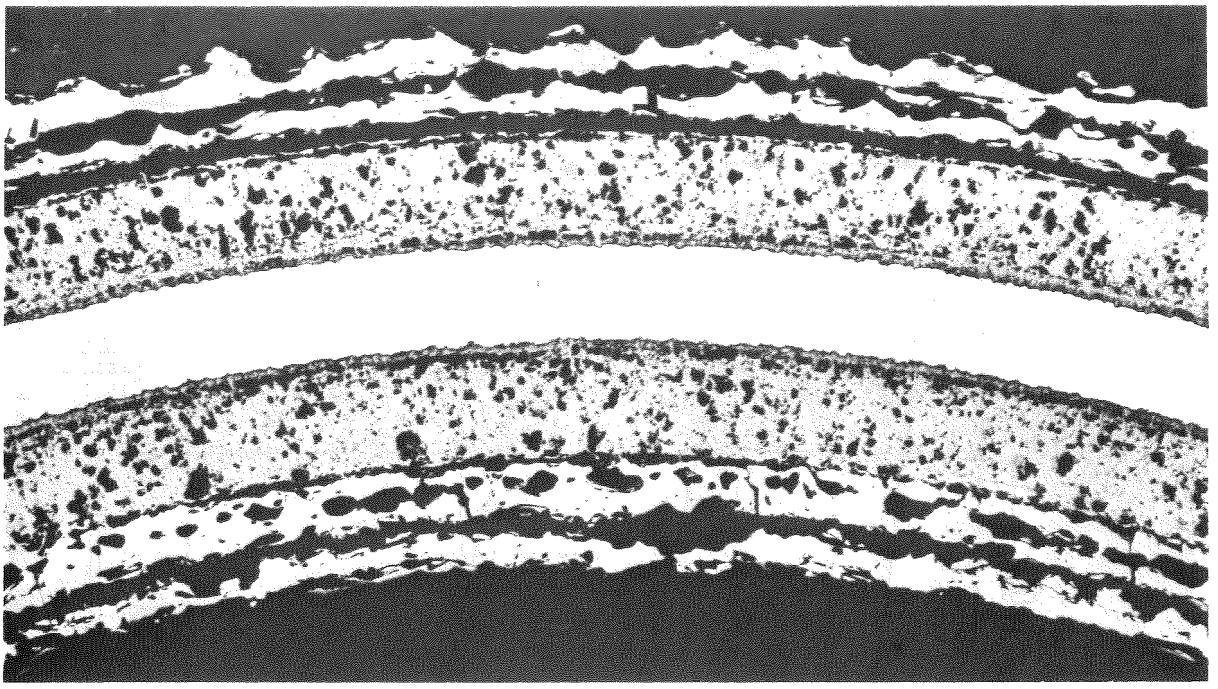

a)

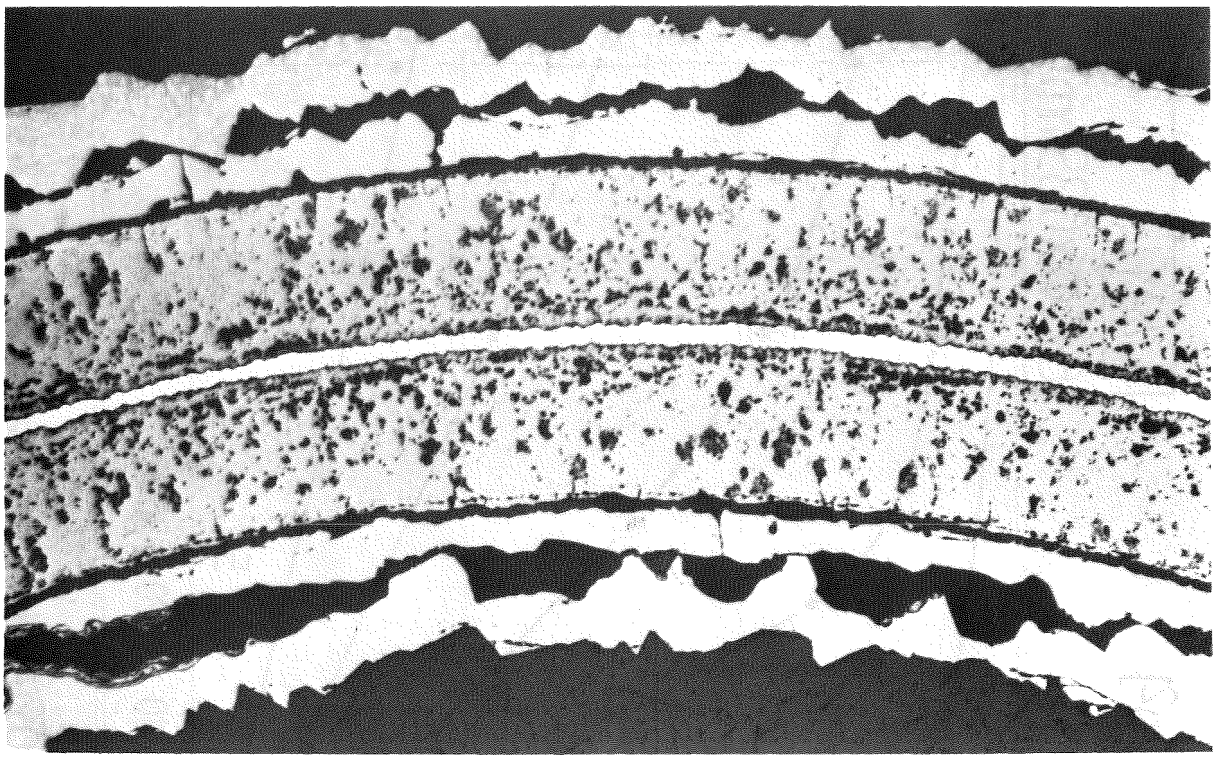

b)

⟷ = 100 µm

Fig. 12

Steam Oxidation of Ferritic-Martensitic Stainless Steel No.1.4914, a) 30min,1100°C, b) 60min,1100°C

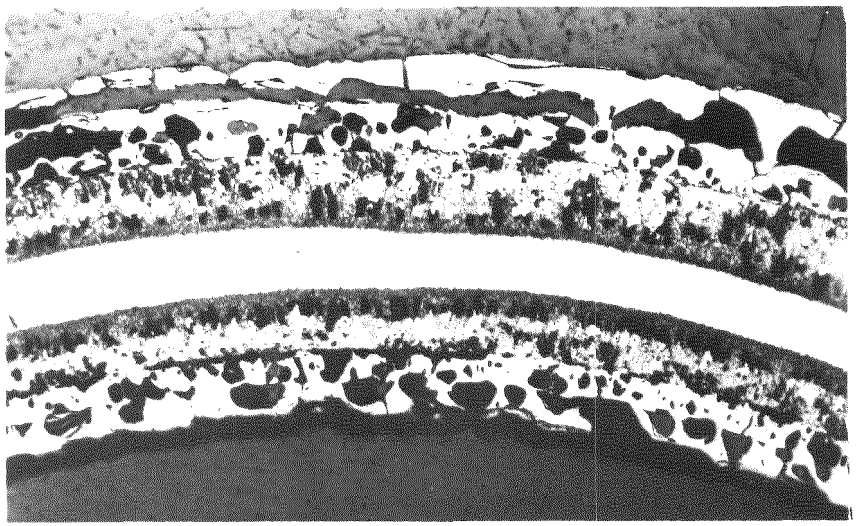

2,5 min

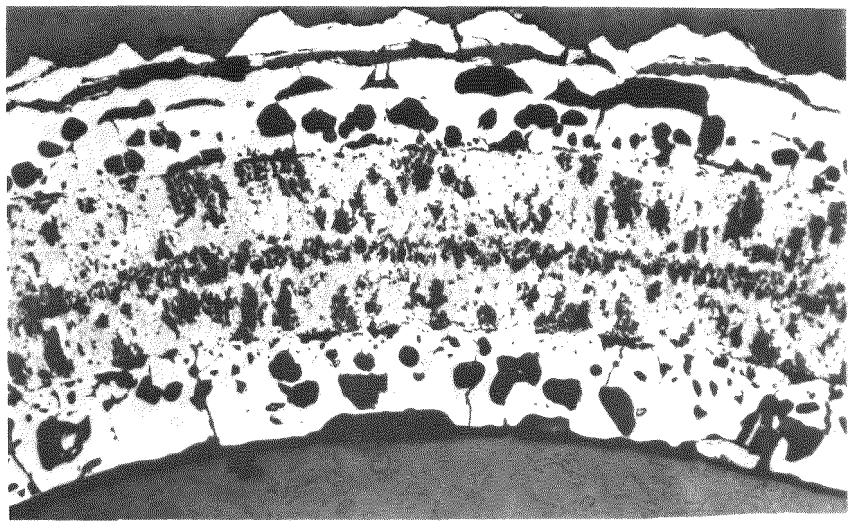

5 min

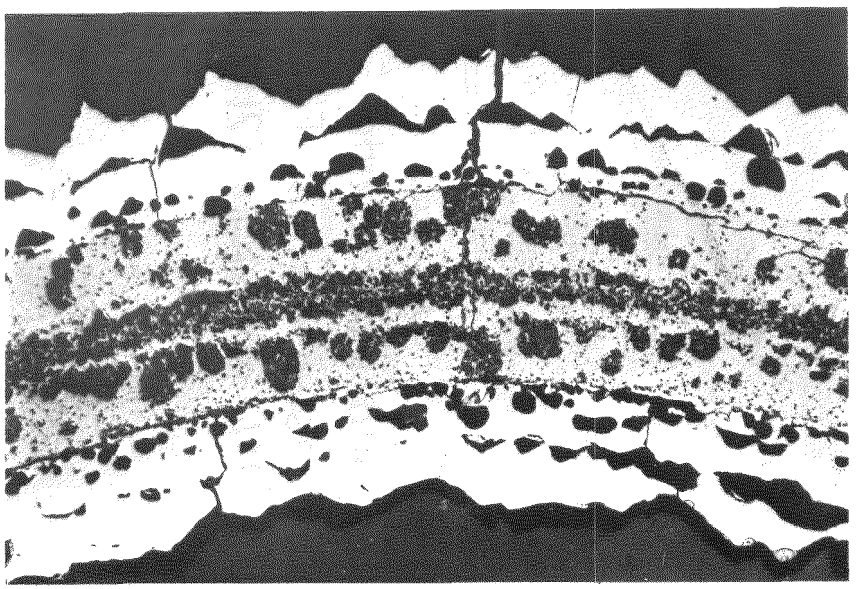

10 min

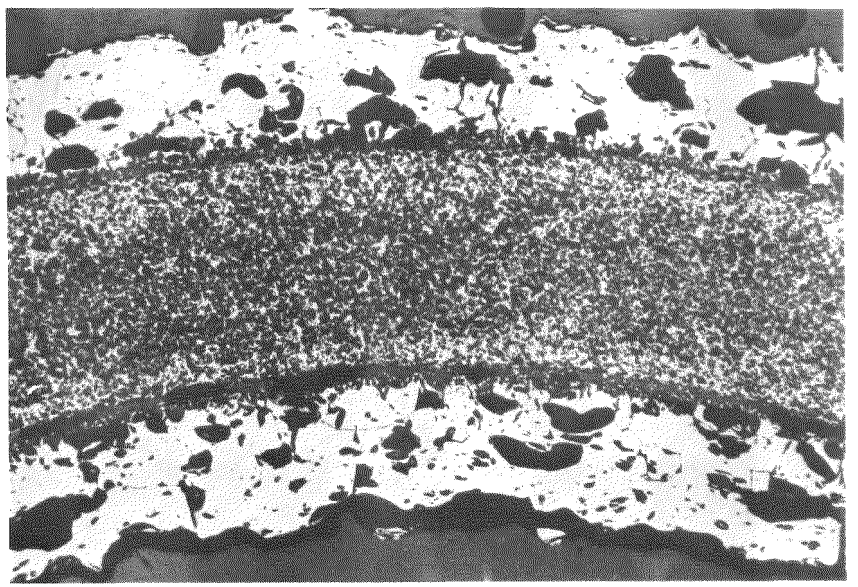

20 min

⟝ 100 µm

KfK

Fig. 13

Steam Oxidation of Mat. No. 1.4914 under LWR-Accident Conditions (2,5-20 min, 1300°C)

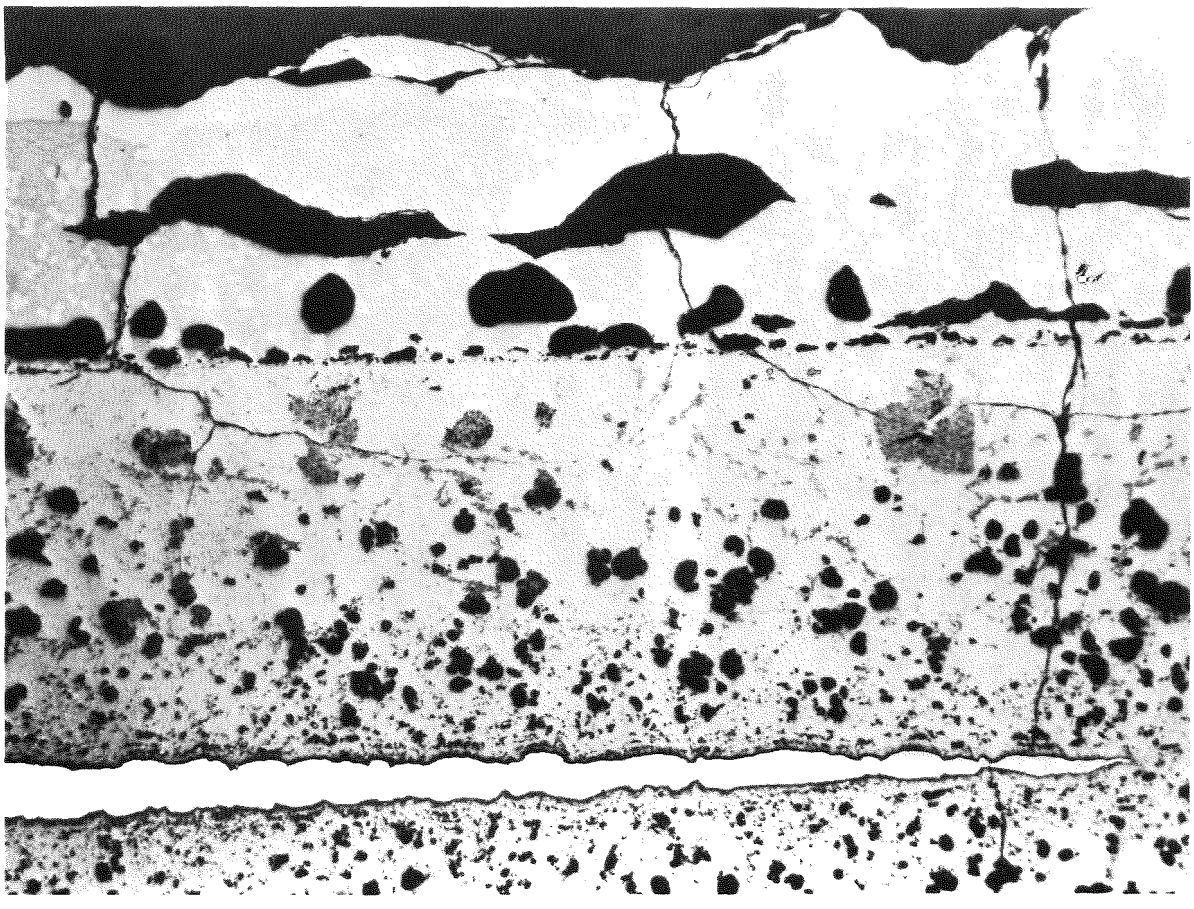

Fig. 14

Outer and Inner Oxide Scale after nearly Total Wall Consumption of Ferritic-Martensitic Steel No. 1.4914 in Steam (2h,1200°C)

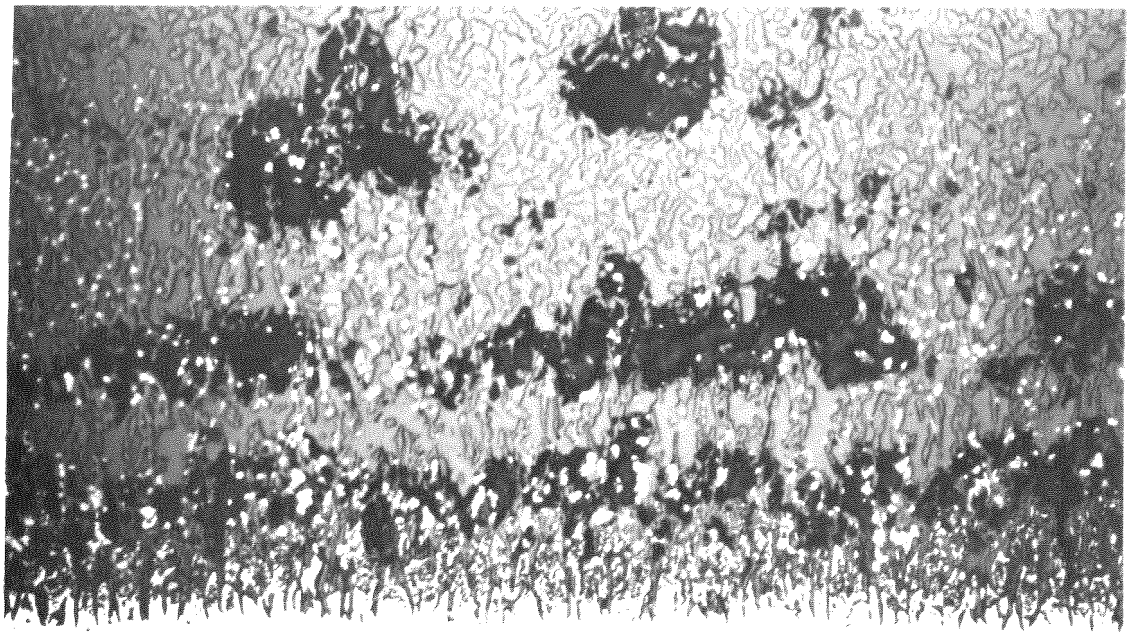

a) 2.5min, 1300°C ⟷ 20µm

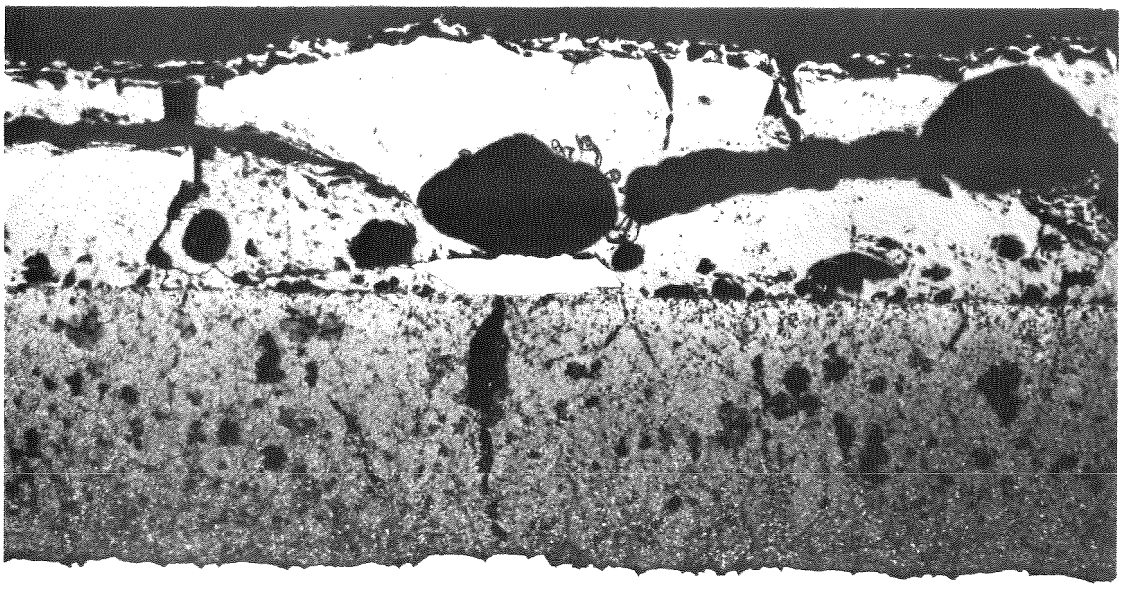

b) 2h, 1100°C ⟷ 100µm

Fig. 15

HT-Steam Oxidation of Ferritic-Martensitic Stainless Steel No. 1.4914
a) Metallic particles within the inner scale
b) Pt-marker on the borderline outer/inner scale

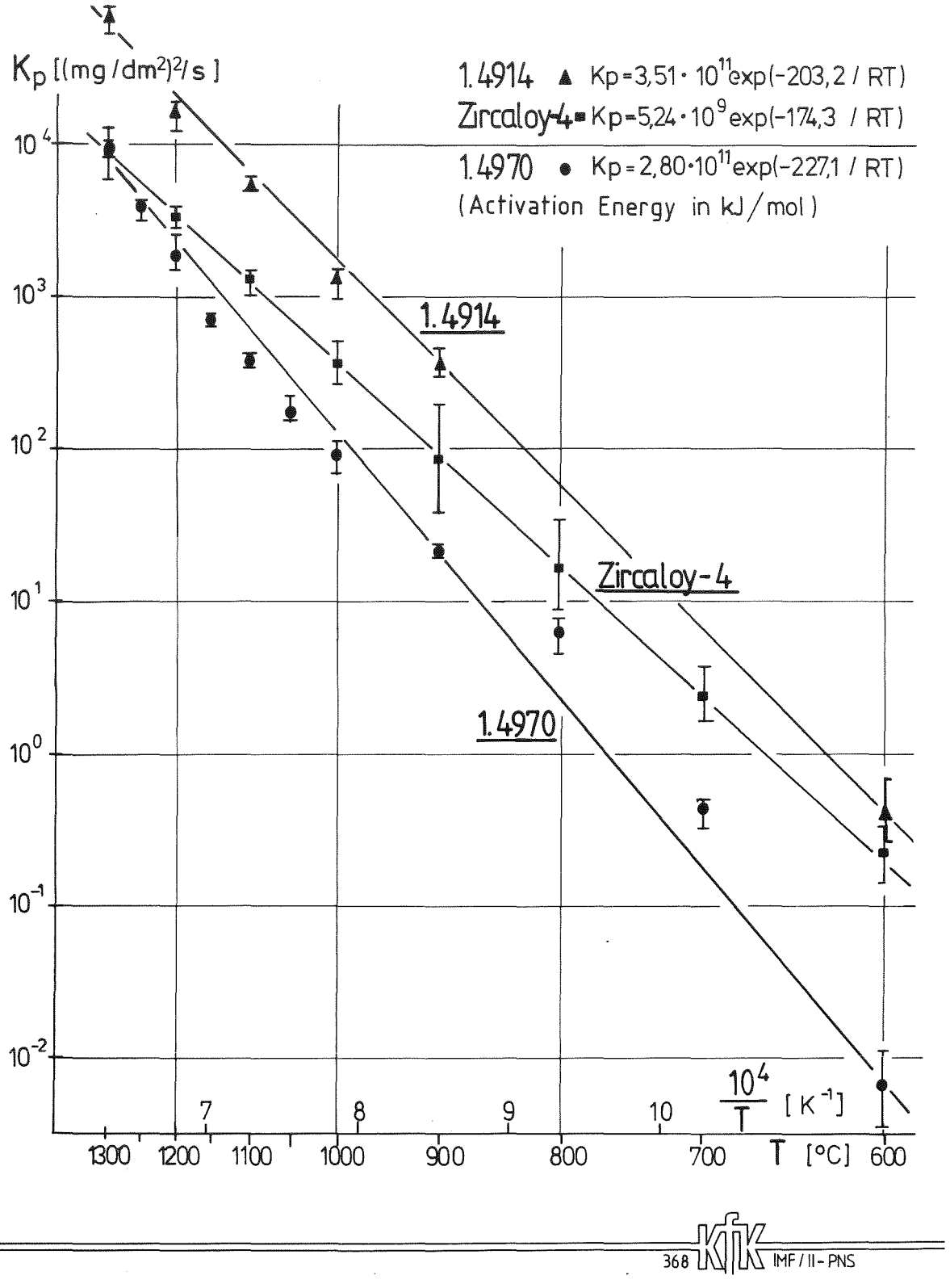

Fig. 16

Arrhenius Diagram of Mass Increase by Steam Oxidation of Mat. No. 1.4914, Zircaloy-4 and Mat. No. 1.4970 (6h, 600-1300°C)

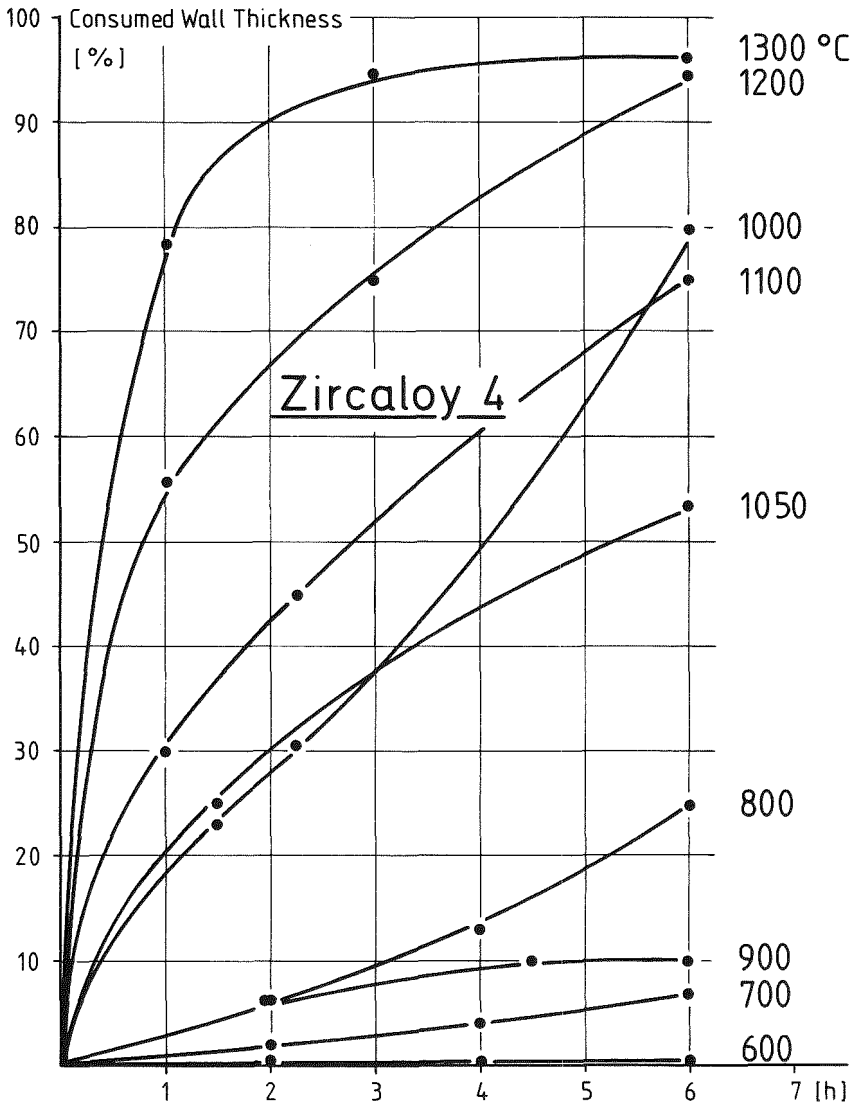

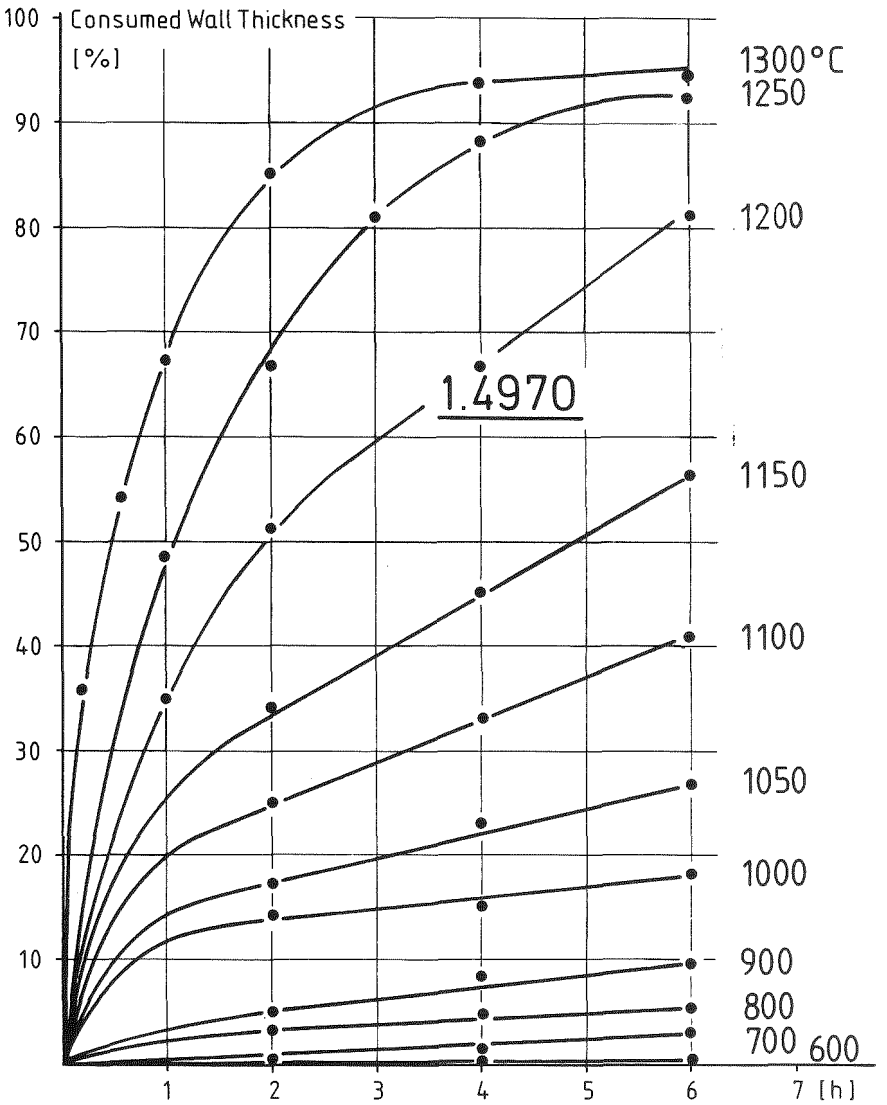

Fig. 17

Comparison of HT - Steam Oxidation of Zircaloy 4 and Austenitic Stainless Steel No. 1.4970 . (Double-Sided Exposure of Tubing: Zry 4 0,725 mm, SS 0,5 mm Wall Thickn.)

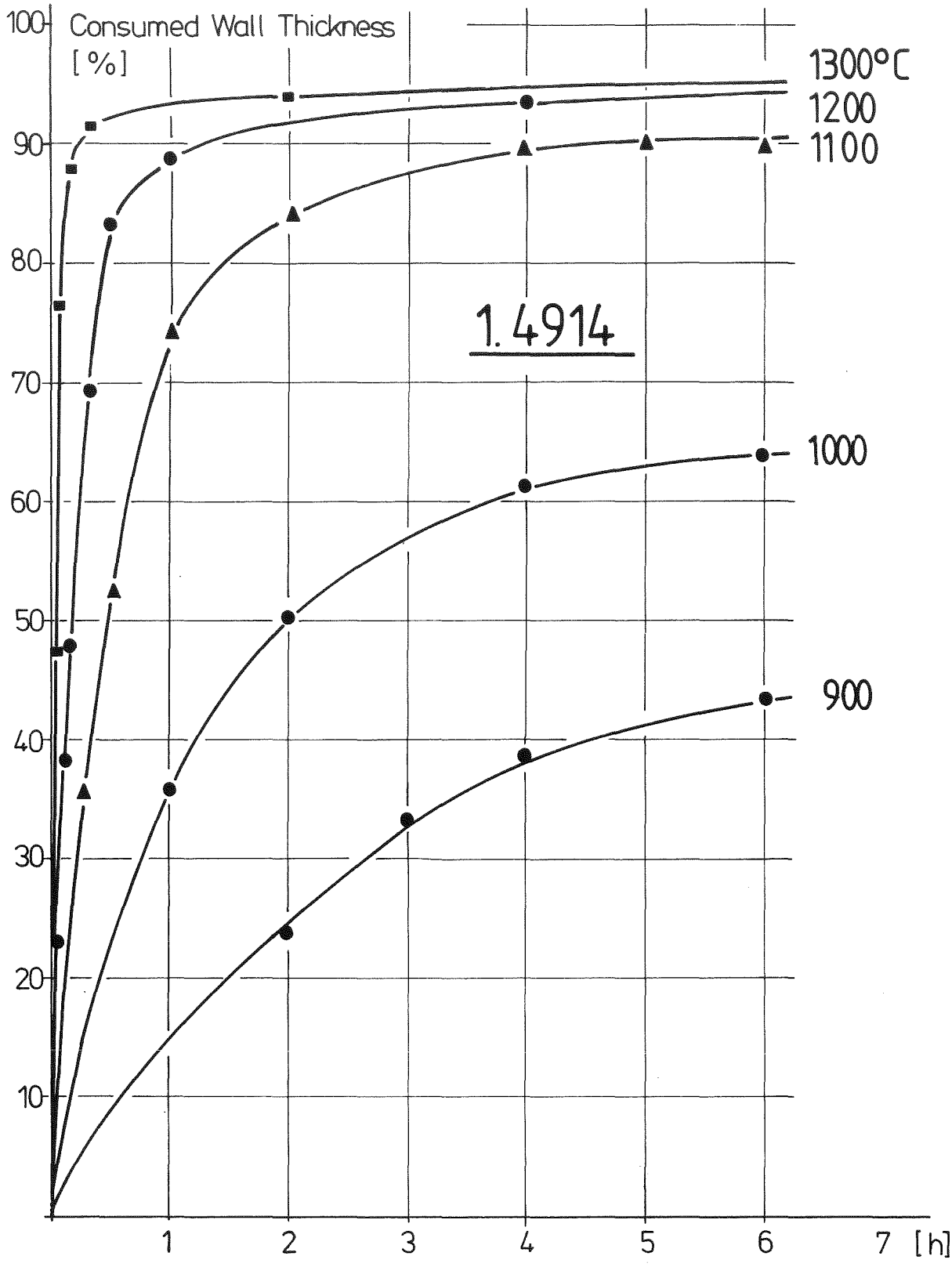

Fig. 18

Wall Consumption of Ferritic-Martensitic Stainless Steel No. 1.4914 by HT-Steam Oxidation as Function of Time and Temperature. Double-Sided Exposure of 0.38 mm Tubing

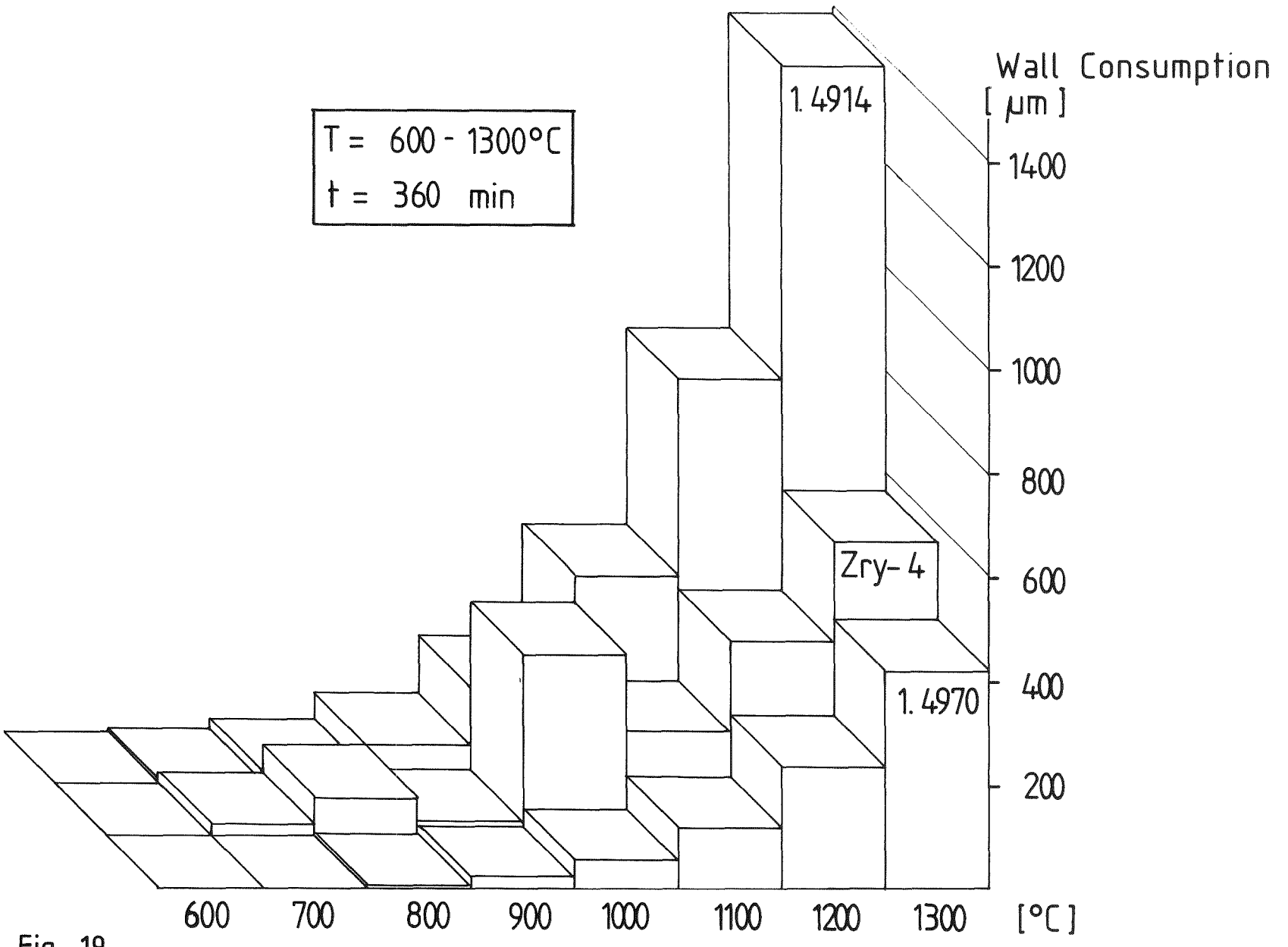

Fig. 19

Comparison of Steam Oxidation Behavior of Mat. No. 1.4914, Zircaloy-4 and Mat. No. 1.4970 when Double-Sided Oxidized at 600-1300°C under Unlimited Wall Dimensions